Impact of physical parameterizations on wind simulation with WRF V3.9.1.1 under stable conditions at PBL gray-zone resolution: a case study over the coastal regions of North China

Entao Yu[1,2], Rui Bai[1,3], Xia Chen[4,5], Lifang Shao[4]

[1] Nansen-Zhu International Research Centre, Institute of Atmospheric Physics, Chinese Academy of Sciences, Beijing, China
[2] Collaborative Innovation Center on Forecast and Evaluation of Meteorological Disasters (CIC-FEMD), Nanjing University of Information Science & Technology, Nanjing, China
[3] University of Chinese Academy of Science (UCAS), Beijing, China
[4] Hebei Climate Center, Shijiazhuang, China
[5] Hebei Key Laboratory for Meteorology and Eco-environment, Shijiazhuang, China

Correspondence to: Entao Yu (yuet@mail.iap.ac.cn) and Xia Chen (chenxia1218@sina.com)

Abstract. Reliable simulation of wind fields under stable weather conditions is vital to prevent air pollution. In this study, we investigate how different physical parameterizations impact simulated near-surface wind at 10-meter height over the coastal regions of North China using the Weather Research and Forecasting (WRF) model with a horizontal grid spacing of 0.5 km. We performed 640 ensemble simulations using multiple combinations of 10 planetary boundary layer (PBL), 16 microphysics (MP), and four shortwave-longwave radiation (SW-LW) schemes. Model performance is evaluated using measurements from weather station observations. The results show that the WRF model can reproduce the temporal variation of wind speed in a reasonable way. The simulated wind speed is most sensitive to the PBL schemes, followed by SW-LW schemes and MP schemes. Among all PBL schemes, the MYJ scheme shows the best temporal correlation with the observed wind speed, while the YSU scheme has the lowest model bias. Dudhia−RRTM and MYDM7 show the best model performances out of all SW-LW and MP schemes, respectively, the interactions among schemes also have large influences on wind simulation. Further investigation indicates that model sensitivity is also impacted by ocean proximity and elevation. For example, for coastal stations, MYNN shows the best correlation with observations among all PBL schemes, while Goddard shows the smallest bias out of SW-LW schemes, these results are different from that of inland stations. In general, WRF simulates wind speed less accurately for coastal stations compared to inland stations, and error metrics (bias and root mean square error) tend to degrade with increasing elevation. The WRF model shows worse performance in simulating wind direction under stable conditions over the study area, with lower correlation scores compared to wind speed. Our results indicate the role parameterizations play in wind simulation under stable weather conditions and provide a valuable reference for further research in the study area and nearby regions.

1 Introduction

Megacities that experience rapid urbanization and economic development also commonly suffer from a simultaneous decline in air quality (Ulpiani, 2021). For example, many haze events have been reported in the Beijing, Tianjin, and Hebei regions of North China over the past few decades. Haze-related weather and associated high concentrations of fine particulate matter have negative impacts on public health and the environment (Wang and Mauzerall, 2006). These events can significantly disrupt economic growth, as demonstrated by the severe haze events that occurred over North China in January 2013 (Zhang et al., 2014; Zhang et al., 2015; Cai et al., 2017). The haze events are most frequent in boreal winter and are closely related to local weather conditions, with haze forming in regions with low wind speeds (Li et al., 2015; Wang et al., 2021). Projections of future climate change suggest that global temperatures will increase, and the frequency of conducive weather conditions to severe haze is projected to increase substantially in response to the climate change, which in turn may increase the frequency of haze event over North China (Cai et al., 2017), however, numerical models always show large bias in wind prediction over China (Gao et al., 2016b; Zhao et al., 2016; Pan et al., 2021), thus it is crucial to improve wind prediction under stable weather conditions in order to minimize associated economic losses and environmental impacts.

In recent years, numerical models have been used extensively to study the weather and climate over China, as they have high spatial and temporal resolutions, and employ sophisticated physical parameterization schemes that can reproduce detailed atmospheric and land surface processes (Wang et al., 2011; Zhou et al., 2019; Kong et al., 2021). However, these models mostly focus on temperature or precipitation, and only a few studies have attempted to simulate winds over China (Li et al., 2019; Xia et al., 2019; Pan et al., 2021). Meanwhile, numerical models inherently involve many sources of uncertainty, as they cannot resolve all processes in the real world; instead, parameterizations are needed to represent the effect of key physical processes, such as radiative transfer, turbulent mixing, and moist convection that occur at the sub-grid scale. Different physical parameterization schemes depict natural phenomena to different degrees of accuracy and choosing appropriate combinations is important, as it strongly influences the model results (Yu et al., 2011; Gómez-Navarro et al., 2015; Stegehuis et al., 2015; Gao et al., 2016b; Yang et al., 2017; Taraphdar et al., 2021).

The impact of the planetary boundary layer (PBL) scheme on wind simulation has been studied for many years, as PBL scheme plays a critical role in modulating mass, energy, and moisture fluxes between the land and atmosphere, which in turn influences the simulation of low-level temperatures, cloud formation, and wind fields (Jiménez and Dudhia, 2012; Gómez-Navarro et al., 2015; Gonçalves-Ageitos et al., 2015; Falasca et al., 2021; Gholami et al., 2021). A lot of studies indicate an overestimation of wind speed in WRF simulations with different PBL schemes (Jiménez and Dudhia, 2012; Carvalho et al., 2014a, b; Pan et al., 2021; Gholami et al., 2021; Dzebre and Adaramola, 2020), for example, Gómez-Navarro et al. (2015) investigate the sensitivity of the WRF model to PBL scheme by simulating wind storms over complex terrain at a horizontal grid spacing of 2 km. In that study, the WRF model is configured with the Mellor-Yamada-Janjic (MYJ) scheme and overestimates wind speed by up to 100%, however, the bias is significantly reduced when the non-local scheme developed at Yonsei University (YSU) is used instead, the YSU scheme also shows good model skill in simulating winds over the northeastern Iberian

Peninsula, Persian Gulf, Tyrrhenian coast, and western Argentina (Jiménez and Dudhia, 2012; Puliafito et al., 2015; Falasca et al., 2021; Gholami et al., 2021). There are also some studies suggesting MYNN and ACM2 are more appropriate for wind simulations (Carvalho et al., 2014b; Chang et al., 2015; Prieto-Herráez et al., 2021; Rybchuk et al., 2021).

The performance of wind simulation is also affected by the choice of cloud microphysics (MP) parameterizations. Cloud microphysical processes, such as moisture evaporation and condensation, can affect thermodynamic and dynamic interactions in the atmosphere (Rajeevan et al., 2010; Santos-Alamillos et al., 2013; Li et al., 2020), then affect the vertical distribution of heat and wind fields close to the surface. Cheng et al. (2013) report that predictions of summer wind speed in northern Colorado are strongly affected by the choice of MP parameterizations.

Another factor influencing wind simulation is the choice of radiation parameterizations, which include shortwave radiation and longwave radiation (SW-LW) schemes. Differences in surface radiation intensities can generate thermal contrasts in regions with complex topography, which in turn affect local and low-level wind distribution patterns (Santos-Alamillos et al., 2013).

The interactions among physical parameterizations are also vital to wind simulation, as they may alter the processes of atmosphere-land interactions, radiation transport, and moist convection, and amplify the uncertainties in wind prediction. The impact of parameterization scheme combination on WRF performance has been investigated in previous studies (Santos-Alamillos et al., 2013; Fernández-González et al., 2018), Fernández-González et al. (2018) report that there is no single combination of schemes that performs best during all weather conditions. Most of the aforementioned studies considered a small number of parameterization schemes, to the best of our knowledge, the sensitivity of parameterizations on wind simulation has not been explored in a systematic way in China. In this study, we systematically evaluate the performance of a large number of parameterization combinations, including PBL, MP, and SW-LW schemes. The investigation is conducted using the WRF model at a grid spacing of 0.5 km, which belongs to the PBL "gray zone" resolution that is too fine to utilize mesoscale turbulence parameterizations and too coarse for large-eddy-simulation (LES) schemes to resolve turbulent eddies (Shin and Hong, 2015; Honnert et al., 2016). Our main objective is to identify a set of configurations of the WRF model that can best reproduce wind fields under stable weather conditions over North China, which experienced many haze events during the past few years. This study addresses the following research themes: (1) quantify the sensitivity of wind simulation to different parameterizations under stable weather conditions, and (2) refine optimized configurations with the best performance in reproducing winds under stable weather conditions over North China. These results would provide a valuable evaluation of WRF performance using a large number of simulations with different physical parameterizations, and be helpful in the wind and air quality forecasts in the study area and other coastal regions of China under stable weather conditions.

This paper is structured as follows: section 2 describes the model setup and the evaluation data, model results are reported in section 3, discussion and concluding remarks are given in sections 4 and 5.

2. Data and methods

2.1. The stable weather event in 2019

The study area is located in the central section of the "Bohai Economic Rim", which is bordered to the southeast by the Bohai Sea and to the northwest by the Yan Mountains (Figure 1a). This region traditionally hosts heavy industry and manufacturing businesses and is a significant region of economic growth and development in North China (Song et al., 2020; Zhao et al., 2020). Air quality in this area has declined over the past decades, and the frequency of winter haze events has increased due to increased pollutant emissions and favorable stable weather conditions with lower wind speed (Gao et al., 2016a; Cai et al., 2017). For instance, during the heavy fog and haze event over eastern China in January 2013, an anomalous southerly wind in the lower troposphere caused by the weak East Asian winter monsoon weakened the synoptic forcing and extent of vertical mixing in the atmosphere, thus increasing the stability of air in the boundary layer and the local concentration of hazes (Zhang et al., 2014). During 11-15 January 2019, a severe haze event occurred in the study area, the peak PM2.5 and PM10 concentrations exceeded 279 μg/m3 and 357 μg/m3 in Tangshan city, and 282 μg/m3 and 358 μg/m3 in Qinhuangdao city, respectively, the locations of the two cities can be found in Figure 1. Figure 2 depicts the distribution of geopotential height, winds, and cloud fraction during the study period, geopotential height and winds are from the ERA5 dataset (Hersbach et al., 2020), and the cloud fractions are from satellite observations of CLARA (CM SAF cLoud, Albedo and surface Radiation) product family (Karlsson et al., 2021). Figure 2 indicates that a weak high-pressure system persisted from 11 to 13 January 2019, along with weak southwest wind in the study area, which would transport warm and wet air to the study area (Gao et al., 2016a), creating a favorable moisture condition for stable conditions and inhibiting pollutants dispersal (Zhang et al., 2014; Hua and Wu, 2022). Then the high-pressure system was replaced by strong northwest wind from 14 to 15 January 2019. The CLARA observations indicate cloud fraction exceeding 60% on 12 January at the study area, while for the rest of the time, cloud fraction is low. This stable event is used to investigate the impact of physical parameterizations of the WRF model.

2.2 Model configurations

WRF model (version 3.9.1.1) with an advanced research WRF (ARW) core is used in this study, which is a non-hydrostatic atmospheric model with terrain-following vertical coordinates (Skamarock et al., 2008). The simulations contain three one-way nested domains with grid spacing of 8 km, 2 km, and 0.5 km for D01, D02, and D03, respectively (Figure 1b). The computational domains are based on a Lambert conformal conic projection centered at 38.5°N and 120°E, with 360 × 480, 381 × 381, and 341 × 421 grid points for D01, D02, and D03, respectively. The evaluations are based on the innermost domain, which covers the coastal and surrounding regions of North China (Figure 1a). The simulation domain has 65 vertical levels, and the eta values for the first 10 levels are 0.996, 0.988, 0.978, 0.966, 0.956, 0.946, 0.933, 0.923, 0.912, and 0.901, this ensures that sufficient model levels exist within the PBL at any time.

The ERA5 reanalysis dataset, which has a horizontal resolution of 0.25° and 38 vertical levels, is used to provide the initial and boundary conditions for WRF simulations. The WRF model is initialized at 00:00 UTC (08:00 in local time) on 9 January

2019, with the first 40 hours treated as the spin-up period. Firstly, the default physical parameterization schemes (Table 2) are applied in the WRF simulation for the outer two domains (D01 and D02), and then the output of D02 is used to drive inner domain simulations with different combinations of PBL, MP, and SW-LW schemes (see section 2.3). This approach helps to isolate the impacts of parameterization within the inner domain from changes in boundary forcing (Yang et al., 2017). All the simulations apply the Noah land surface model with multi-parameterization options (Noah-MP, Yang et al., 2011; Niu et al., 2011) as the land surface parameterization scheme. The lateral boundary conditions and sea surface temperature are updated every three hours using the ERA5 reanalysis data, and the frequency of wind retrieved from WRF output is hourly, which matches the frequency of observations in the study area.

2.3 Experimental design

The WRF model contains different parameterization schemes that represent different physical processes. Further, every scheme in the model has many parameters, such that a model can range from being simple and efficient to sophisticated and computationally costly. In this study, a systematic evaluation of parameterizations is achieved by considering 10 PBL, 16 MP, and four LW-SW schemes, which produce 640 (i.e., $10 \times 16 \times 4$) combinations in total.

The parameterization schemes investigated in this study are listed in Table 1. As the horizontal grid spacing of 0.5 km is within the PBL gray zone resolution, both PBL and LES assumptions are imperfect, we test both PBL and LES schemes in this study. For the LES configuration, the 1.5-order turbulence kinetic energy closure model is used to parameterize motion at the sub-grid scale (Deardorff, 1985). For the YSU scheme, topographic correction for surface winds is included to represent extra drag from sub-grid topography and enhanced flow at hilltops (Jiménez and Dudhia, 2012). The option for top-down mixing driven by radiative cooling is also turned on during the integration. For the rest of the PBL schemes, the default configurations are chosen. The atmospheric surface layer (SL) is the lowest part of the atmospheric boundary layer, of which the parameterizations are used to quantify surface heat and moisture fluxes in the land surface model and surface stress in the PBL schemes. In the current generation of WRF, the SL schemes are tied to the PBL schemes. In this study, ETA, QNSE, MYNN, Pleim-Xiu, and TEMF schemes are chosen separately for PBL schemes of MYJ, QNSE, MYNN, ACM2, and TEMF. The revised MM5 scheme (Jimenez et al., 2012) is used for the rest PBL schemes.

Sixteen MP schemes are applied in this study (Table 1), Lin, WSM3, WSM5, ETA, WSM6, Goddard, SBU, and NSSL1 schemes are the single-moment bulk microphysical scheme, which predicts only the mixing ratios of hydrometeors (i.e., cloud ice, snow, graupel, rain, and cloud water) by assuming particle size distributions. The other eight schemes (Thompson, MYDM7, Morrison, CMA, WDM6, NSSL2, ThompsonAA and P3) use a double-moment approach, predicting not only mixing ratios of hydrometeors but also number concentrations. Among them, two types of hydrometeors are included in WSM3 (cloud water and rain), three types of hydrometeors are included in ETA (cloud water, rain, and snow) and P3 (cloud water, rain, and ice), four types of hydrometeors are included in WSM5 and SBU (cloud water, rain, ice, and snow), five types of hydrometeors are included in Lin, WSM6, Goddard, Thompson, Morrison, CAM, WDM6 and ThompsonAA (cloud water, rain, ice, snow, and graupel), six types of hydrometeors are included in MYDM7, NSSL1, and NSSL2 (cloud water, rain, ice,

snow, graupel, and hail). According to the user's guide of ARW (Skamarock et al., 2008), WSM6, Thompson, Morrison, WDM6, NSSL1, and NSSL2 are suitable for high-resolution simulations.

Four SW-LW combinations are applied in this study (Table 1), Dudhia is a simple and efficient shortwave radiation scheme for clouds and clear-sky absorption and scattering; RRTM provides efficient look-up tables for longwave radiation; CAM SW-LW schemes are derived from the CAM3 model used in CCSM3, and allows modeling of aerosols and trace gases. RRTMG is a scheme that utilizes Monte Carlo independent column approximation (MCICA) method of random cloud overlap.

2.4 Observational data and evaluation metrics

Observations from weather stations across the study region are used to evaluate the performance of the model. These stations are operated by the China Meteorology Administration (CMA), and report wind speed and direction at an altitude of 10 m. In this study, we use two-minute-averaged wind speed at hourly frequency. All data are screened before analysis in order to remove stations with data showing spurious jumps (e.g., wind speed jumps to 0 m/s due to frozen sensor). After this filtering, 105 out of 132 weather stations (Figure 1a) remained, including 89 inland stations and 16 coastal stations. The results of WRF are directly compared with observations made at each weather station, which is achieved by using the model result that is geographically closest to the weather station under consideration. Although some errors are introduced when performing these comparisons, they are systematic and shared by all simulations, and therefore have minor effects on the evaluation of model performances.

Several metrics are employed for evaluating the performance of each model configuration, including the Pearson's correlation coefficient (CORR), BIAS, root mean square error (RMSE), and Taylor skill score (T). They are defined as follows:

$$CORR = \frac{\sum_{i=1}^{N}(M_i-\overline{M})(O_i-\overline{O})}{\sqrt{\sum_{i=1}^{N}(M_i-\overline{M})^2 \cdot \sum_{i=1}^{N}(O_i-\overline{O})^2}}$$

$$BIAS = \frac{1}{N}\sum_{i=1}^{N}(M_i - O_i)$$

$$RMSE = \sqrt{\frac{1}{N}\sum_{i=1}^{N}(M_i - O_i)^2}$$

$$T = \frac{2(1+CORR)}{\left(SD+\frac{1}{SD}\right)^2}$$

Here, M is the value of the model output, O is the value of the observation, N is the number of observations, and SD is the ratio of simulated to observed standard deviation. A higher Taylor skill score indicates a more accurate simulation (Gan et al., 2019).

The difference in wind direction was calculated as follows:

$$\Delta = \begin{cases} M - O, & when\ |M-O| \le 180° \\ (M-O)\left(1-\frac{360}{|M-O|}\right), & when\ |M-O| > 180° \end{cases}$$

The correlation between simulated and measured angles is determined by a circular correlation coefficient, and the mean of angular is calculated using vector notation approach, circular correlation coefficient is calculated as follows:

$$CORR = \frac{\sum_{i=1}^{N} sin(\alpha_i - \overline{\alpha}) sin(\beta_i - \overline{\beta})}{\sqrt{\sum_{i=1}^{N} sin^2(\alpha_i - \overline{\alpha}) sin^2(\beta_i - \overline{\beta})}}$$

Here, α and β are simulated and observed wind direction angles, respectively.

3. Results

3.1 Impacts of physical parameterizations

3.1.1 PBL

Figure 3a shows the time series of observed wind speed in local time and the corresponding simulations using different PBL schemes. The WRF model generally reproduces the temporal variation of observed wind speed in the study area with exaggeration; in particular, the shift from low to high wind speed on 14 January 2019 is reproduced by all schemes except for QNSE, with which the wind speed change is considerably larger than with all other schemes during the simulation period. Almost all the PBL schemes overestimate wind speed by 1 m/s, however, for the QNSE scheme, the largest overestimation exceeds 10 m/s during the daytime on 11 and 15 January 2019. Further comparison shows that the difference between simulation and observation is lower during 11-13 January 2019 using the LES scheme, while YSU shows a lower difference during 14-15 January 2019. In addition, the spread within the PBL schemes is larger on 15 January 2019, partly due to high wind speed (> 4 m/s) or the general error growth in the model.

The statistics of CORR, BIAS, and RMSE are illustrated in Figure 3b-d, MYJ shows the best CORR score of 0.96, MYNN, ACM2 and UW are slightly worse according to this verification score. YSU is the best scheme in terms of BIAS and RMSE with the values of 0.45 m/s and 0.61 m/s, flowed by MYNN (0.55 m/s and 0.70 m/s). The ranges of statistic scores across the 105 stations are also illustrated in Figure 3, for the schemes except for QNSE, the range of CORR is 0.2-0.8, the range of BIAS is -2-2 m/s, and the range of RMSE is 0.7-2.5 m/s. Further comparison indicates that the CORR scores for individual stations are lower than the ensemble mean, and the BIAS and RMSE are larger than the ensemble mean. For the QNSE scheme, the maximum BIAS and RMSE scores for individual stations exceed 10 m/s and 16 m/s, indicating that it has problems in reproducing wind speed under stable conditions over the study area.

Figure 4 shows the wind roses during 11-15 January 2019 from observation and simulations with different PBL schemes, as well as the statistic scores. Observations indicate that during the study period, wind is mostly from southwest to northwest direction (225-330°), while simulations with different PBL schemes produce primarily southwest wind (200-270°), indicating an anticlockwise bias of wind direction over the study area under stable conditions. Further comparison indicates that all PBL schemes strongly overestimate the speed of north wind compared to the observations, which is the main cause of positive bias

in wind speed (Figure 3). The CORR scores of wind direction (0.42-0.59) are notably lower than that of wind speed, indicating the degraded performance of WRF in wind direction simulation. LES shows the best CORR score of 0.59, while TEMF shows the best BIAS and RMSE scores of -11° and 56°. Considering the large model bias in wind speed, simulations with the QNSE scheme (64 in total) are omitted from further investigation in order that these anomalous data do not affect our overall analysis.

3.1.2 MP

Figure 5 shows the time series of wind speed from the observation and simulations with different MP schemes. The simulations are similar, especially during 14-15 January 2019. The spread among simulations with different MP schemes is smaller than that with different PBL schemes, indicating that wind speed is less sensitive to the MP schemes. The CORR scores are generally the same for all the MP schemes, while MYDM7 is the best scheme according to BIAS and RMSE scores, followed by P3 and ETA. The range of statistic scores across the stations is similar within different MP schemes, which provides a further indication of the low sensitivity of wind speed to MP schemes.

The sensitivity of wind direction to the MP schemes is also low, as the wind roses from simulations with different MP schemes are very similar (Figure 6). WDM6, NSSL2 and ThompsonAA show the best CORR score of 0.52, followed by Thompson and CAM5. Meanwhile, WSM3 is the best scheme according to the BIAS score, and ThompsonAA is the best scheme according to the RMSE score.

3.1.3 Radiation

Figure 7 shows the time series of observed and simulated wind speed, the ensemble spread among different SW-LW schemes is larger than that with different MP schemes, but smaller than that with different PBL schemes, which indicates that simulated wind speed is more sensitive to the SW-LW schemes than the MP schemes and less sensitive to the PBL schemes. Further comparison indicates that RRTMG and CAM show a strong overestimation of wind speed, especially for the peak values during the daytime. Simulations with the Dudhia-RRTM schemes reduce the bias and are closer to the observations. The CORR scores are the same for the SW-LW schemes, and Dudhia-RRTM is the best scheme according to BIAS and RMSE scores, followed by Goddard.

Figure 8 shows the wind roses during 11-15 January 2019 from simulations with different SW-LW schemes and the corresponding statistic scores. In simulations, wind is mostly from the southwest direction during the study period, which is different from the observation. According to the CORR score, Dudhia-RRTM is the best scheme with the highest value (0.55), meanwhile, the RRTMG scheme shows the best BIAS of -16°, and Dudhia-RRTM shows the best RMSE of 61°.

3.1.4 Interactions among parameterization schemes

Interactions among physical parameterizations also play an important role in wind simulation. Since it is not possible to show all possible combinations of PBL, MP, and SW-LW schemes in this study, the results of interactions between PBL and SW-LW schemes are selected as an example, which is illustrated in Figure 9. The MP schemes applied in the simulations are

MYDM7 and P3, given that they show better performance in earlier investigations (see Section 3.1.2), thus for each MP scheme, a total of 36 simulations (excluding QNSE) are evaluated and the results are expected to be consistent with evaluations using other MP schemes. For wind speed simulations with both MYDM7 and P3, MYJ shows the best CORR score, while YSU shows the lowest BIAS and RMSE scores. However, further investigation indicates that YSU shows lower BIAS and RMSE scores only when combined with Dudhia-RRTM or Goddard, when it is applied with RRTMG, the BIAS and RMSE scores show an obvious increasement compared with that with Dudhia-RRTM. For the wind direction simulation, the combination of LES and Dudhia-RRTM shows the best CORR score, while the combination of LES and TEMF is the best according to BIAS and RMSE scores. Thus, the choice of suitable scheme combination also plays an important role in determining the model performance in the simulation of wind speed and direction. Overall, for BIAS and RMSE scores of wind speed, within each SW-LW group, the same PBL scheme ranks best (e.g., for wind-speed RMSE, no matter which PBL scheme, Dudhia-RRTM and Goddard are always best), and within each PBL scheme, the same SW-LW group ranks best, this indicates that a systematic variation of parameterizations is not necessary. However, for wind-speed CORR and wind direction, this pattern is not always consistent. For example, for wind-direction BIAS, the best SW-LW group depends on the choice of PBL scheme (e.g., for MYDM7 with TEMF, Dudhia-RRTM is best; for P3 MP scheme with TEMF, RRTMG is best), this indicates that a systematic variation of parameterizations is important when focusing on these variables.

3.1.5 WRF configurations with the best individual performance

To determine the WRF configuration with the best individual performance, Taylor skill scores are calculated for wind speed within all simulations, the scores range from 0.2 to 1.0, with the best 10 WRF configurations having similar scores of about 1.0. The timeseries and statistics are illustrated in Figure 10. The best 10 configurations have in common that they use the same PBL and SW-LW schemes, namely YSU and Dudhia-RRTM. Due to the slight differences between models using different MP schemes, the 10 best performing WRF configuration only vary in MP schemes. This indicates a large impact of PBL and SW-LW on wind speed simulation compared with MP schemes, and highlights the best performance of YSU and Dudhia-RRTM. Since Taylor skill score considers both correlation (CORR) and standard deviation (SD), the best scheme (i.e., WDM6) is not the scheme that has the best CORR (i.e., Goddard), BIAS (i.e., MYDM7 and ETA), or RMSE (Goddard, NSSL1, MYDM7 and ETA). In fact, there is no scheme that has all the best scores of CORR, BIAS and RMSE. Thus, model ensemble is needed to improve the performance. Figure 10 also illustrates the ensemble of different number of simulations, as well as a super ensemble of all 576 simulations (excluding QNSE). The result indicates that ensemble mean of four simulations with WDM6, Goddard, NSSL1 and MYDM7 shows the best BIAS and RMSE scores. Figure 10 also shows the time series of wind speed from ensemble of 4 (ENS4) and all 576 simulations (ENSall), the spread of ENS4 is significantly lower than that of ENSall, and ENS4 shows smaller difference with the observation compared to ENSall. According to the statistic scores, ENS4 reduces model bias by approximately half compared to ENSall.

3.2 Performance dependency on ocean proximity and elevation

Land surface conditions can affect the partitioning of sensible and latent heat fluxes, which impacts local low-level circulation patterns and wind distribution (Yu et al., 2013; Barlage et al., 2016). The weather stations in the study region were classified into different groups according to the ocean proximity and elevation. The effects of these parameters on the model results are presented below.

3.2.1 Ocean proximity

Figure 11 compares the results of wind speed for coastal stations (closer than 5 km from the shoreline, 89 stations in total) and inland stations (over 5 km from the shoreline, 16 stations in total), the locations of these stations are shown in Figure 1a. For both coastal and inland stations, the ensemble spread is the largest among the PBL schemes, followed by SW-LW and MP schemes, which is consistent with the results of the previous analysis in this study. WRF reproduces the timeseries of wind speed reasonably, with a larger overestimation for inland stations. Further comparison indicates that the ensemble spread is larger for coastal stations compared with inland stations, especially among the MP schemes during 11-13 January 2019 with lower wind speed. As such, in addition to physical parameterizations, model performance is also influenced by ocean proximity, and WRF simulates wind speed less accurately for coastal stations compared to inland stations.

The statistic scores are also illustrated in Figure 11, the CORR scores are consistently lower and the BIAS and RMSE scores are generally worse for coastal stations compared to inland stations, which indicates degraded model performance for coastal stations. This degradation may be caused by the uncertainties from the prescribed SST in our simulation, which may require a better description of atmosphere-ocean coupling process in future model development.

Our comparison indicates that the parameterization schemes with the best performance for inland stations are generally consistent with those of previous investigations in this study, considering most of the stations are inland stations (89 out of 105 stations), this result is not surprising, however, for coastal stations, the result is different. For instance, MYNN shows the best CORR score among the PBL schemes, while LES (YSU) shows the best BIAS (RMSE) score. For SW-LW schemes, Goddard shows the best scores of CORR, BIAS and RMSE, while Dudhia-RRTM ranks worst according to the CORR score.

3.2.2 Elevation

Figure 12 shows the comparison for stations with different elevation (e.g., < 50m, 51 stations in total; >50 & < 250m, 36 stations in total; < 250m, 19 stations in total). Observation shows that peak wind speed decreases with increasing elevation during the study period; for example, the peak observed wind speed of high-elevation stations (>250 m) is 1.5 m/s slower than that of low-elevation stations (<50 m). However, the peak simulated wind speed is generally similar for stations with different elevation, which bring larger model error for the high-elevation stations. As shown by the statistic scores, for each PBL, MP and SW-LW schemes, CORR generally decreases with increasing elevation, while BIAS and RMSE scores increase with elevation, thus the evaluation metrics tend to degrade with increasing elevation under stable conditions over the study area.

Further comparison indicates that for different parameterization types, the scheme with the best performance is generally similar with different elevations, e.g., for the PBL schemes, MYJ is always best at all elevation categories according to the CORR score, and YSU is always best according to the BIAS and RMSE scores.

4. Discussion

In order to evaluate atmospheric properties that are crucial for air quality under stable conditions and investigate what drives the differences in wind speed, we compare the simulated wind field from the simulation with the best Taylor skill score (i.e., using YSU, Dudhia-RRTM and WDM6 schemes) to the station observations, meanwhile, the same simulation but with QNSE PBL scheme (i.e., using QNSE, Dudhia-RRTM and WDM6 schemes) is used for comparison between the PBL schemes. In addition, the impact of different options in the YSU scheme and land surface model is also discussed in this section.

4.1 Spatial distribution of wind field

Figure 13 compares the spatial distribution of observed and simulated wind fields during the study period, we choose 14:00 in local time as an example. The simulation with the best Taylor skill score is referred to as YSU, and the simulation using QNSE, Dudhia-RRTM and WDM6 schemes is referred to as QNSE. YSU generally reproduces the wind field in the study area, especially in terms of wind speed. For example, the observed wind speed is lower on 13 January 2019, with values lower than 2 m/s in many stations, while on 15 January 2019, the observed wind speed is higher than 4 m/s in most of the stations. In the simulation with YSU, wind speed is about 2 m/s on 13 January 2019 and higher than 4 m/s on 15 January 2019 over the study area, which is close to the observation. On the contrary, simulation with QNSE fails to reproduce the distribution of wind speed, and shows strong overestimation, especially over the mountain areas of the study area, for example, the peak wind speed in simulation with QNSE exceeds 20 m/s on 15 January 2019, which is more than five times greater than the observation, this overestimation is consistent with the large positive bias in previous investigation of Figure 3. For the wind-direction simulation, YSU shows degraded performance compared to wind speed, and generally fails to reproduce the wind-direction distribution for most of the stations, QNSE also fails to do so.

4.2 Vertical profile of wind speed

Figure 14 shows the observed and simulated vertical profile of wind speed at 08:00 and 20:00 during the study period, the location of the sounding station is illustrated in Figure 1. YSU reproduces the vertical structure of wind speed reasonably, with slightly larger model bias above the height of 15 km. Within the low levels below 2.5 km, simulated wind speed from the YSU scheme is close to the observation, with the bias lower than 2.5 m/s in most cases. Meanwhile, QNSE shows worse performance in reproducing the vertical structure of wind speed, with significant larger model bias compared to YSU. for example, QNSE overestimates the low-level (< 2.5 km) wind speed by about 10 m/s at 20:00 on 11 January 2019, and overestimate wind speed by 20 m/s at 20:00 on 11 January 2019. It is interesting to note that the simulation with QNSE is pretty similar to that with

YSU at 08:00 during the study period, indicating that large difference between YSU and QNSE only occurs at specific time during the study period, which is also revealed in Figure 3a.

4.3 Impact of options in the YSU scheme

The impact of different options in YSU on wind-speed simulation is illustrated in Figure 15, the simulation with the best Taylor skill score in previous investigation is selected and referred to as YSU, three extra simulations with top-down mixing option turning off (No_mix), topographic correction option turning off (No_topo), and both options turning off (No_topo_mix) are conducted for comparison. The simulated wind speed increases when we turn off the individual or both options, which enlarges the overestimation of wind speed under stable conditions in our study (Figure 15a). Further investigation indicates that turning off the two options in YSU mainly degrades model performance with worse evaluation metrics, for example, the BIAS score increases from 0.36 m/s to 0.67 m/s in No_topo, to 0.43 m/s in No_mix, and to 0.69 m/s in No_topo_mix, the RMSE scores show similar degradation to BIAS by turning off the options in YSU.

4.4 Impact of land surface model

Figure 16 shows the evaluation of different land surface parameterizations with the same model configuration as the simulation with the best Taylor skill score, the land surface models (LSM) considered are the five-layer thermal diffusion scheme (SLAB, Dudhia, 1996), the Noah scheme (NOAH, Chen and Dudhia, 2001), the Rapid Update Cycle scheme (RUC, Smirnova et al., 2000), the Noah-MP scheme (NOAHMP), and the Community Land Model Version 4 scheme (CLM4, Lawrence et al., 2011). The simulations with different LSMs reproduce the timeseries of wind speed well, with larger spread during 14-15 January 2019 (Figure 16a). NOAHMP shows the best CORR score of 0.94, CLM4 and NOAH are slightly worse according to this score. Meanwhile, according to the RMSE score, NOAHMP is the best scheme, followed by RUC and NOAH. In addition, RUC and NOAHMP show better BIAS scores than the other LSMs. Thus, NOAHMP shows the best performance among different LSMs in wind-speed simulation under stable conditions in this study, however, the large difference among LSMs indicates that we should take land surface parameterizations into consideration in future studies.

4.5 Impact of choice of ensemble

In this study, CORR, BIAS and RMSE are used as verification scores, CORR is a measure of the strength and direction of the linear relationship between simulation and observation, BIAS is a measure of the mean difference between simulation and observation, and RMSE is the square root of the average of the set of squared differences between simulation and observation, thus each of these metrics gives a partial view of the model performance, and some schemes perform best according to one metric and worst according to another in our previous investigation.

As none of the schemes is the best according to all the scores, model ensemble is used to provide optimizing model performance, at the same time, model ensemble also provides probabilistic evaluation of the simulations and ensembles with narrow spread are often overconfident. The ensemble mean of 576 simulations in our study shows the best CORR score (0.94 in Figure 10)

in wind-speed simulation, however, this best CORR score is also result of single-model simulation with Goddard MP scheme. At the same time, the best wind-speed BIAS score (0.33 m/s) is result of the single-model simulation with MYDM7 or ETA, and the best RMSE score (0.52 m/s) is result of either the single-model simulation with Goddard, NSSL1, MYDM7, or the ensemble using the 3, 4 or 5 best simulations. Thus, model ensemble does not always provide the best performance, and model post-processing, especially the bias correction techniques are needed to be taken into consideration, which can significantly reduce the systematic errors in model simulation. In addition, the PBL schemes play a dominant role in wind simulation, further tuning of the parameters within the PBL schemes, such as turbulent kinetic energy (TKE) dissipation rate, TKE diffusion factor, and turbulent length-scale coefficients is needed. Finally, it is worth pointing out that the presented findings in this study could be unique to the meteorological setup of the event, the location, the input dataset, the domain setup, and other unchanged parameterization types or model settings.

5. Conclusion remarks

In this study, we investigate wind simulations during a relatively long period of stable conditions when a haze event affected North China. Surface meteorological observations are used to evaluate the WRF model's ability to reproduce the evolution of winds during the event. A number of WRF sensitivity experiments (640 in total) are conducted, altering the PBL, radiation, and microphysical schemes to determine the sensitivity of wind speed and direction simulations to model physical parameterizations. Further investigations considering the ocean proximity and elevation are conducted to provide deeper insight into the factors that influence model sensitivities.

In general, the WRF model reproduces the temporal variation of wind speed over the study area well, the spread in wind speed is largest within the PBL schemes tested, followed by SW-LW, and then MP schemes. The wind direction is notably worse reproduced by WRF compared to wind speed. This result is consistent with the findings of previous simulations performed in other locations (Dzebre and Adaramola, 2020; Gómez-Navarro et al., 2015; Santos-Alamillos et al., 2013).

Among all PBL schemes, MYJ shows the best CORR score of 0.96, MYNN, ACM2 and UW are slightly worse according to this score. YSU is the best scheme according to the BIAS and RMSE scores (0.45 m/s and 0.61 m/s), flowed by MYNN (0.55 m/s and 0.70 m/s). For the SW-LW and MP schemes, the CORR scores are similar, and Dudhia−RRTM and MYDM7 show the best model performance out of all SW-LW and MP schemes according to the BIAS and RMSE scores. The interactions among physical parameterization schemes also play an important role in wind simulations, as the best verification scores can only be achieved by certain combination of schemes. The ensemble mean of all the simulations shows the highest CORR core in wind speed, while the best 10 simulations show much better performance than the ensemble in terms of BIAS and RMSE.

The schemes with the best performance for inland stations are consistent with the results of all stations, as the majority of stations are inland stations, however, for coastal stations, MYNN is the best scheme among all PBL schemes according to CORR, while LES (YSU) shows the best BIAS (RMSE) score. For SW-LW schemes, Goddard shows the best scores of CORR, BIAS and RMSE, while Dudhia-RRTM ranks worst according to the CORR score. The schemes with the best performance

are similar with different elevations for different parameterization types, however, model performance tends to degrade with increasing elevation.

A large number of WRF simulations altering the PBL, MP, and radiation schemes are conducted in this study to investigate the model sensitivity of wind speed and direction to parameterizations under stable conditions over North China, the horizontal resolution of 0.5 km belongs to the PBL gray zone, which has rarely been used in previous simulation studies in China, thus the results of this study provide a valuable reference for other simulations over North China.

Code and data availability

The Weather Research and Forecasting (WRF) model is freely available online and can be downloaded from the page: https://github.com/wrf-model/WRF. The ERA5 data are available at ECMWF (https://www.ecmwf.int/en/forecasts/datasets/reanalysis-datasets/era5). The CLARA product are available at Climate Data Store (https://cds.climate.copernicus.eu/cdsapp#!/dataset/satellite-cloud-properties?tab=overview). The observations and model's hourly output upon which this work is based are available at Zonodo (https://doi.org/10.5281/zenodo.6505423), all the results can also be obtained from yuet@mail.iap.ac.cn.

Author contributions

EY conceptualized the study and conducted the simulations. The analysis was carried out by all the authors. The original draft of the paper was written by EY, all the authors took part in the edition and revision of it.

Competing interests

The authors declare that they have no conflict of interest.

Acknowledgements

This work was supported by the National Natural Science Foundation of China (No. 42088101 and 42075168), the Technology Innovation Guidance Program of Hebei Province (No. 21475401D) and the National Key Research and Development Program of China (No. 2020YFF0304401). The simulation was supported by the National Key Scientific and Technological Infrastructure project Earth System Numerical Simulation Facility (EarthLab).

References

Angevine, W. M., Jiang, H., and Mauritsen, T.: Performance of an eddy diffusivity–mass flux scheme for shallow cumulus boundary layers, Mon Weather Rev, 138, 2895-2912, 2010.

Barlage, M., Miao, S., Chen, F.: Impact of physics parameterizations on high-resolution weather prediction over two Chinese megacities, Journal of Geophysical Research: Atmospheres 121, 4487-4498, 2016.

Bougeault, P. and Lacarrere, P.: Parameterization of orography-induced turbulence in a mesobeta--scale model, Mon Weather Rev, 117, 1872-1890, 1989.

Bretherton, C. S. and Park, S.: A new moist turbulence parameterization in the Community Atmosphere Model, Journal of Climate, 22, 3422-3448, 2009.

Cai, W., Li, K., Liao, H., Wang, H., and Wu, L.: Weather conditions conducive to Beijing severe haze more frequent under climate change, Nat. Clim. Chang., 7, 257-262, 10.1038/nclimate3249, 2017.

Carvalho, D., Rocha, A., Gómez-Gesteira, M., and Silva Santos, C.: Offshore wind energy resource simulation forced by different reanalyses: Comparison with observed data in the Iberian Peninsula, Applied Energy, 134, 57-64, https://doi.org/10.1016/j.apenergy.2014.08.018, 2014a.

Carvalho, D., Rocha, A., Gómez-Gesteira, M., and Silva Santos, C.: Sensitivity of the WRF model wind simulation and wind energy production estimates to planetary boundary layer parameterizations for onshore and offshore areas in the Iberian Peninsula, Applied Energy, 135, 234-246, https://doi.org/10.1016/j.apenergy.2014.08.082, 2014b.

Chang, R., Zhu, R., Badger, M., Hasager, C. B., Xing, X., and Jiang, Y.: Offshore Wind Resources Assessment from Multiple Satellite Data and WRF Modeling over South China Sea, Remote Sens-Basel, 7, 467-487, 2015.

Chen, F., and Dudhia, J.: Coupling an advanced land-surface hydrology model with the Penn State-NCAR MM5 modeling system. Part I: Model description and implementation, Mon. Weather Rev., 129, 569–585, 2001.

Chen, S. H. and Sun, W. Y.: A one-dimensional time dependent cloud model, Journal of the Meteorological Society of Japan. Ser. II, 80, 99-118, 2002.

Cheng, W. Y. Y., Liu, Y., Liu, Y., Zhang, Y., Mahoney, W. P., and Warner, T. T.: The impact of model physics on numerical wind forecasts, Renewable Energy, 55, 347-356, https://doi.org/10.1016/j.renene.2012.12.041, 2013.

Collins, W. D., Rasch, P. J., Boville, B. A., Hack, J. J., McCaa, J. R., Williamson, D. L., Kiehl, J. T., Briegleb, B., Bitz, C., and Lin, S.-J.: Description of the NCAR community atmosphere model (CAM 3.0), NCAR Tech. Note NCAR/TN-464+ STR, 226, 1326-1334, 2004.

Deardorff, J.: Sub-grid-scale turbulence modeling. Advances in Geophysics, Academic Press, 28, 337–343, https://doi.org/10.1016/S0065-2687(08)60193-4, 1985.

Dudhia, J.: Numerical study of convection observed during the winter monsoon experiment using a mesoscale two-dimensional model, Journal of Atmospheric Sciences, 46, 3077-3107, 1989.

Dudhia, J.: A multi-layer soil temperature model for MM5, in 6th PSU/NCAR Mesoscale Model Users' Workshop, Boulder, Colo, 49–50, 1996.

Dzebre, D. E. K. and Adaramola, M. S.: A preliminary sensitivity study of Planetary Boundary Layer parameterisation schemes in the weather research and forecasting model to surface winds in coastal Ghana, Renewable Energy, 146, 66-86, https://doi.org/10.1016/j.renene.2019.06.133, 2020.

Eaton, B.: User's guide to the Community Atmosphere Model CAM-5.1, NCAR. URL http://www.cesm. ucar. edu/models/cesm1. 0/cam, 2011.

Falasca, S., Gandolfi, I., Argentini, S., Barnaba, F., Casasanta, G., Di Liberto, L., Petenko, I., and Curci, G.: Sensitivity of near-surface meteorology to PBL schemes in WRF simulations in a port-industrial area with complex terrain, Atmospheric Research, 264, 105824, https://doi.org/10.1016/j.atmosres.2021.105824, 2021.

Fernández-González, S., Martín, M. L., García-Ortega, E., Merino, A., Lorenzana, J., Sánchez, J. L., Valero, F., Rodrigo, J. S.: Sensitivity Analysis of the WRF Model: Wind-Resource Assessment for Complex Terrain, Journal of Applied Meteorology and Climatology, 57(3), 733-753, 2018.

Gan, Y., Liang, X.-Z., Duan, Q., Chen, F., Li, J., and Zhang, Y.: Assessment and Reduction of the Physical Parameterization Uncertainty for Noah-MP Land Surface Model, Water Resources Research, 55, 5518-5538, https://doi.org/10.1029/2019WR024814, 2019.

Gao, M., Carmichael, G. R., Wang, Y., Saide, P. E., Yu, M., Xin, J., Liu, Z., and Wang, Z.: Modeling study of the 2010 regional haze event in the North China Plain, Atmos. Chem. Phys., 16, 1673–1691, 2016a.

Gao, X., Shi, Y., and Giorgi, F.: Comparison of convective parameterizations in RegCM4 experiments over China with CLM as the land surface model, Atmospheric and Oceanic Science Letters, 9, 246-254, 10.1080/16742834.2016.1172938, 2016b.

Gholami, S., Ghader, S., Khaleghi-Zavareh, H., and Ghafarian, P.: Sensitivity of WRF-simulated 10 m wind over the Persian Gulf to different boundary conditions and PBL parameterization schemes, Atmospheric Research, 247, 105147, https://doi.org/10.1016/j.atmosres.2020.105147, 2021.

Gómez-Navarro, J. J., Raible, C. C., and Dierer, S.: Sensitivity of the WRF model to PBL parametrisations and nesting techniques: evaluation of wind storms over complex terrain, Geosci. Model Dev., 8, 3349-3363, 10.5194/gmd-8-3349-2015, 2015.

Gonçalves-Ageitos, M., Barrera-Escoda, A., Baldasano, J. M., and Cunillera, J.: Modelling wind resources in climate change scenarios in complex terrains, Renewable energy, 76, 670-678, 2015.

Hersbach, H., Bell, B., Berrisford, P., Hirahara, S., Horányi, A., Muñoz-Sabater, J., Nicolas, J., Peubey, C., Radu, R., Schepers, D. and Simmons, A.: The ERA5 global reanalysis. Quarterly Journal of the Royal Meteorological Society, 146, 1999-2049, 2020.

Hong, S.-Y. and Lim, J.-O. J.: The WRF single-moment 6-class microphysics scheme (WSM6), Asia-Pacific Journal of Atmospheric Sciences, 42, 129-151, 2006.

Hong, S.-Y., Dudhia, J., and Chen, S.-H.: A revised approach to ice microphysical processes for the bulk parameterization of clouds and precipitation, Mon Weather Rev, 132, 103-120, 2004.

Hong, S., Noh, Y., and Dudhia, J.: A new vertical diffusion package with an explicit treatment of entrainment processes, Mon Weather Rev, 134, 2318-2341, 2006.

Honnert, R., Couvreux, F., Masson, V., Lancz, D.: Sampling the structure of convective turbulence and implications for grey-zone parametrizations, Boundary-Layer Meteorol, 160, 133–156, 2016.

Hua, W., Wu, B.: Atmospheric circulation anomaly over mid- and high-latitudes and its association with severe persistent haze events in Beijing, Atmospheric Research, 277, 106315, 2022.

Iacono, M. J., Delamere, J. S., Mlawer, E. J., Shephard, M. W., Clough, S. A., and Collins, W. D.: Radiative forcing by long-lived greenhouse gases: Calculations with the AER radiative transfer models, Journal of Geophysical Research: Atmospheres, 113, 2008.

Janjić, Z. I.: The step-mountain eta coordinate model: Further developments of the convection, viscous sublayer, and turbulence closure schemes, Mon Weather Rev, 122, 927-945, 1994.

Jiménez, P. A. and Dudhia, J.: Improving the representation of resolved and unresolved topographic effects on surface wind in the WRF model, J Appl Meteorol Clim, 51, 300-316, 2012.

Jimenez, P. A., Dudhia, J., Fidel Gonzalez–Rouco, J., Navarro, J., Montavez J., and Garcia-Bustamante, E.: A revised scheme for the WRF surface layer formulation. Mon. Wea. Rev., 140, 898–918, 2012.

Karlsson, K., Riihelä, A., Trentmann, J., Stengel, M., Meirink, J., Solodovnik, I., Devasthale, A., Manninen, T., Jääskeläinen, E., Anttila, K., Kallio-Myers, V., Benas, N., Selbach, N., Stein, D., Kaiser, J., Hollmann, R.: ICDR AVHRR-based on CLARA-A2 methods, Satellite Application Facility on Climate Monitoring, doi:10.5676/EUM_SAF_CM/CLARA_AVHRR/V002_01, 2021.

Kong, X., Wang, A., Bi, X., Sun, B., and Wei, J.: The hourly precipitation frequencies in the tropical-belt version of WRF: sensitivity to cumulus parameterization and radiative schemes, Journal of Climate, 1-59, 10.1175/jcli-d-20-0854.1, 2021.

Lawrence, D., Oleson, K., Flanner, M., Thornton, P., Swenson, S., Lawrence, P., Zeng, X., Yang, Z., Levis, S., Sakaguchi, K., Bonan, G., Slater, A.: Parameterization improvements and functional and structural advances in Version 4 of the Community Land Model, J. Adv. Model. Earth Syst., 3, M03001, doi:10.1029/2011MS00045, 2011.

Li, J., Ding, C., Li, F., and Chen, Y.: Effects of single- and double-moment microphysics schemes on the intensity of super typhoon Sarika (2016), Atmospheric Research, 238, 104894, https://doi.org/10.1016/j.atmosres.2020.104894, 2020.

Li, M., Tang, G., Huang, J., Liu, Z., An, J., and Wang, Y.: Characteristics of winter atmospheric mixing layer height in Beijing-Tianjin-Hebei region and their relationship with the atmospheric pollution (in Chinese), Enviromental Science, 36, 1935-1943, 10.13227/j.hjkx.2015.06.004, 2015.

Li, S., Sun, X., Zhang, S., Zhao, S., and Zhang, R.: A Study on Microscale Wind Simulations with a Coupled WRF–CFD Model in the Chongli Mountain Region of Hebei Province, China, Atmosphere-Basel, 10, 731, 2019.

Lim, K.-S. S. and Hong, S.-Y.: Development of an effective double-moment cloud microphysics scheme with prognostic cloud condensation nuclei (CCN) for weather and climate models, Mon Weather Rev, 138, 1587-1612, 2010.

Lin, Y. and Colle, B. A.: A new bulk microphysical scheme that includes riming intensity and temperature-dependent ice characteristics, Mon Weather Rev, 139, 1013-1035, 2011.

Mansell, E. R., Ziegler, C. L., and Bruning, E. C.: Simulated electrification of a small thunderstorm with two-moment bulk microphysics, Journal of Atmospheric Sciences, 67, 171-194, 2010.

Matsui, T., Zhang, S. Q., Lang, S. E., Tao, W.-K., Ichoku, C., and Peters-Lidard, C. D.: Impact of radiation frequency, precipitation radiative forcing, and radiation column aggregation on convection-permitting West African monsoon simulations, Clim Dyn, 55, 193-213, 2020.

Mesinger, F.: Forecasting upper tropospheric turbulence within the framework of the Mellor-Yamada 2.5 closure, Res. Activ. Atmos. Oceanic Mod., 1993.

Milbrandt, J. and Yau, M.: A multimoment bulk microphysics parameterization. Part I: Analysis of the role of the spectral shape parameter, Journal of the atmospheric sciences, 62, 3051-3064, 2005.

Mirocha, J., Lundquist, J., and Kosović, B.: Implementation of a nonlinear subfilter turbulence stress model for large-eddy simulation in the Advanced Research WRF model, Mon Weather Rev, 138, 4212-4228, 2010.

Mlawer, E. J., Taubman, S. J., Brown, P. D., Iacono, M. J., and Clough, S. A.: Radiative transfer for inhomogeneous atmospheres: RRTM, a validated correlated-k model for the longwave, Journal of Geophysical Research: Atmospheres, 102, 16663-16682, 1997.

Morrison, H. and Milbrandt, J. A.: Parameterization of cloud microphysics based on the prediction of bulk ice particle properties. Part I: Scheme description and idealized tests, Journal of Atmospheric Sciences, 72, 287-311, 2015.

Morrison, H., Thompson, G., and Tatarskii, V.: Impact of cloud microphysics on the development of trailing stratiform precipitation in a simulated squall line: Comparison of one-and two-moment schemes, Mon Weather Rev, 137, 991-1007, 2009.

Nakanishi, M. and Niino, H.: Development of an improved turbulence closure model for the atmospheric boundary layer, Journal of the Meteorological Society of Japan. Ser. II, 87, 895-912, 2009.

Niu, G. Y., Yang, Z. L., Mitchell, K. E., Chen, F., Ek, M. B., Barlage, M., Kumar, A., Manning, K., Niyogi, D., and Rosero, E.: The community Noah land surface model with multiparameterization options (Noah-MP): 1. Model description and evaluation with local-scale measurements, Journal of Geophysical Research: Atmospheres, 116, 2011.

Pan, L., Liu, Y., Roux, G., Cheng, W., Liu, Y., Hu, J., Jin, S., Feng, S., Du, J., and Peng, L.: Seasonal variation of the surface wind forecast performance of the high-resolution WRF-RTFDDA system over China, Atmospheric Research, 259, 105673, https://doi.org/10.1016/j.atmosres.2021.105673, 2021.

Pleim, J. E.: A combined local and nonlocal closure model for the atmospheric boundary layer. Part I: Model description and testing, J Appl Meteorol Clim, 46, 1383-1395, 2007.

Prieto-Herráez, D., Frías-Paredes, L., Cascón, J. M., Lagüela-López, S., Gastón-Romeo, M., Asensio-Sevilla, M. I., Martín-Nieto, I., Fernandes-Correia, P. M., Laiz-Alonso, P., Carrasco-Díaz, O. F., Sáez-Blázquez, C., Hernández, E., Ferragut-Canals, L., and González-Aguilera, D.: Local wind speed forecasting based on WRF-HDWind coupling, Atmospheric Research, 248, 105219, https://doi.org/10.1016/j.atmosres.2020.105219, 2021.

Puliafito, S. E., Allende, D. G., Mulena, C. G., Cremades, P., and Lakkis, S. G.: Evaluation of the WRF model configuration for Zonda wind events in a complex terrain, Atmospheric Research, 166, 24-32, https://doi.org/10.1016/j.atmosres.2015.06.011, 2015.

Rajeevan, M., Kesarkar, A., Thampi, S. B., Rao, T. N., Radhakrishna, B., and Rajasekhar, M.: Sensitivity of WRF cloud microphysics to simulations of a severe thunderstorm event over Southeast India, Ann. Geophys., 28, 603-619, 10.5194/angeo-28-603-2010, 2010.

Rogers, E., Black, T., Ferrier, B., Lin, Y., Parrish, D., and DiMego, G.: Changes to the NCEP Meso Eta Analysis and Forecast System: Increase in resolution, new cloud microphysics, modified precipitation assimilation, modified 3DVAR analysis, NWS Technical Procedures Bulletin, 488, 15, 2001.

Rybchuk, A., Optis, M., Lundquist, J. K., Rossol, M., and Musial, W.: A Twenty-Year Analysis of Winds in California for Offshore Wind Energy Production Using WRF v4.1.2, Geosci. Model Dev. Discuss., 2021, 1-41, 10.5194/gmd-2021-50, 2021.

Santos-Alamillos, F. J., Pozo-Vázquez, D., Ruiz-Arias, J. A., Lara-Fanego, V., and Tovar-Pescador, J.: Analysis of WRF Model Wind Estimate Sensitivity to Physics Parameterization Choice and Terrain Representation in Andalusia (Southern Spain), J Appl Meteorol Clim, 52, 1592-1609, 10.1175/jamc-d-12-0204.1, 2013.

Shin, H. H. and Hong, S.: Representation of the subgrid-scale turbulent transport in convective boundary layers at gray-zone resolutions, Mon Weather Rev, 143, 250-271, 2015.

Skamarock, W. C., Klemp, J. B., Dudhia, J., Gill, D. O., Barker, D. M., Wang, W., and Powers, J. G.: A description of the Advanced Research WRF version 3, NCAR Technical note-475+ STR, 2008.

Smirnova, T. G., Brown, J. M., Benjamin, S. G., and Kim D.: Parameterization of cold-season processes in the MAPS land surface scheme, J. Geophys. Res., 105, 4077–4086, doi:10.1029/1999JD901047, 2000.

Song, M., Wu, J., Song, M., Zhang, L., Zhu, Y.: Spatiotemporal regularity and spillover effects of carbon emission intensity in China's Bohai Economic Rim, Science of The Total Environment, 740, 140184, 2020.

Stegehuis, A. I., Vautard, R., Ciais, P., Teuling, A. J., Miralles, D. G., and Wild, M.: An observation-constrained multi-physics WRF ensemble for simulating European mega heat waves, Geosci. Model Dev., 8, 2285-2298, 10.5194/gmd-8-2285-2015, 2015.

Sukoriansky, S., Galperin, B., and Perov, V.: Application of a new spectral theory of stably stratified turbulence to the atmospheric boundary layer over sea ice, Boundary-layer meteorology, 117, 231-257, 2005.

Tao, W.-K., Simpson, J., and McCumber, M.: An ice-water saturation adjustment, Mon Weather Rev, 117, 231-235, 1989.

Taraphdar, S., Pauluis, O. M., Xue, L., Liu, C., Rasmussen, R., Ajayamohan, R. S., Tessendorf, S., Jing, X., Chen, S., and Grabowski, W. W.: WRF Gray-Zone Simulations of Precipitation Over the Middle-East and the UAE: Impacts of Physical

Parameterizations and Resolution, Journal of Geophysical Research: Atmospheres, 126, e2021JD034648, https://doi.org/10.1029/2021JD034648, 2021.

Thompson, G. and Eidhammer, T.: A study of aerosol impacts on clouds and precipitation development in a large winter cyclone, Journal of the atmospheric sciences, 71, 3636-3658, 2014.

Thompson, G., Field, P. R., Rasmussen, R. M., and Hall, W. D.: Explicit forecasts of winter precipitation using an improved bulk microphysics scheme. Part II: Implementation of a new snow parameterization, Mon Weather Rev, 136, 5095-5115, 2008.

Tiedtke, M.: A comprehensive mass flux scheme for cumulus parameterization in large–scale models. Mon. Wea. Rev., 117, 1779–1800, 1989.

Ulpiani, G.: On the linkage between urban heat island and urban pollution island: Three-decade literature review towards a conceptual framework, Science of The Total Environment, 751, 141727, https://doi.org/10.1016/j.scitotenv.2020.141727, 2021.

Wang, H., Yu, E., and Yang, S.: An exceptionally heavy snowfall in Northeast china: large-scale circulation anomalies and hindcast of the NCAR WRF model, Meteorology and Atmospheric Physics, 113, 11-25, 10.1007/s00703-011-0147-7, 2011.

Wang, T., Zhang, M., and Han, X.: Source Apportionment of PM2.5 during a Heavy Pollution Episode in Qinhuangdao in Winter 2019 Using a Chemical Transport Model, Climatic and Environmental Research (in Chinese), 26, 471-481, 2021.

Wang, X. and Mauzerall, D. L.: Evaluating impacts of air pollution in China on public health: Implications for future air pollution and energy policies, Atmos Environ, 40, 1706-1721, https://doi.org/10.1016/j.atmosenv.2005.10.066, 2006.

Xia, G., Zhou, L., Minder, J. R., Fovell, R. G., and Jimenez, P. A.: Simulating impacts of real-world wind farms on land surface temperature using the WRF model: physical mechanisms, Clim Dyn, 53, 1723-1739, 10.1007/s00382-019-04725-0, 2019.

Yang, B., Qian, Y., Berg, L. K., Ma, P.-L., Wharton, S., Bulaevskaya, V., Yan, H., Hou, Z., and Shaw, W. J.: Sensitivity of Turbine-Height Wind Speeds to Parameters in Planetary Boundary-Layer and Surface-Layer Schemes in the Weather Research and Forecasting Model, Boundary-Layer Meteorology, 162, 117-142, 10.1007/s10546-016-0185-2, 2017.

Yang, Z., Niu, G., Mitchell, K. E., Chen, F., Ek, M. B., Barlage, M., Longuevergne, L., Manning, K., Niyogi, D., and Tewari, M.: The community Noah land surface model with multiparameterization options (Noah-MP): 2. Evaluation over global river basins, Journal of Geophysical Research: Atmospheres, 116, 2011.

Yu, E., Wang, H., Gao, Y., and Sun, J.: Impacts of cumulus convective parameterization schemes on summer monsoon precipitation simulation over China, Acta Meteorologica Sinica, 25, 581-592, 2011.

Yu, E., Wang, H., Sun, J., Gao, Y.: Climatic response to changes in vegetation in the Northwest Hetao Plain as simulated by the WRF model, International Journal of Climatology, 33, 1470-1481, 2013.

Zhang, L., Wang, T., Lv, M., and Zhang, Q.: On the severe haze in Beijing during January 2013: Unraveling the effects of meteorological anomalies with WRF-Chem, Atmos Environ, 104, 11-21, https://doi.org/10.1016/j.atmosenv.2015.01.001, 2015.

Zhang, R., Li, Q., and Zhang, R.: Meteorological conditions for the persistent severe fog and haze event over eastern China in January 2013, Science China Earth Sciences, 57, 26-35, 10.1007/s11430-013-4774-3, 2014.

Zhao, J., Guo, Z., S, Z., Zhao, Z., Xiao, X., Liu, F.: An improved multi-step forecasting model based on WRF ensembles and creative fuzzy systems for wind speed, Applied Energy, 162, 808-826, 2016.

Zhao, Y., Zhou, J., Fan, Y., Feng, M., Zhang, Z.: Economic and environmental impacts of China's imported iron ore transport chain under road-to-rail policy: an empirical analysis based on the Bohai Economic Rim, Carbon Management, 11:6, 653-671, 2020.

Zhou, X., Yang, K., Beljaars, A., Li, H., Lin, C., Huang, B., and Wang, Y.: Dynamical impact of parameterized turbulent orographic form drag on the simulation of winter precipitation over the western Tibetan Plateau, Clim Dyn, 53, 707-720, 10.1007/s00382-019-04628-0, 2019.

635 **Table 1: List of microphysics (MP), planetary boundary layer (PBL), shortwave-longwave radiation (SW-LW) schemes investigated in this study.**

MP	PBL	SW	LW
Purdue Lin (Lin; Chen and Sun, 2002)	LES (Mirocha et al., 2010)	Dudhia (Dudhia, 1989)	RRTM (Mlawer et al., 1997)
WRF single-moment 3-class (WSM3; Hong et al., 2004)	Yonsei University (YSU; Hong et al., 2006)	CAM (Collins et al., 2004)	CAM (Collins et al., 2004)
WRF single-moment 5-class (WSM5; Hong et al., 2004)	Mellor–Yamada–Janjic (MYJ; Janjić, 1994; Mesinger, 1993)	RRTMG (Iacono et al., 2008)	RRTMG (Iacono et al., 2008)
ETA Ferrier (ETA, Rogers et al., 2001)	Quasi-normal scale elimination (QNSE; Sukoriansky et al., 2005)	Goddard (Matsui et al., 2020)	Goddard (Matsui et al., 2020)
WRF single-moment 6-class (WSM6; Hong and Lim, 2006)	Mellor–Yamada Nakanishi Niino 2.5 level TKE (MYNN; Nakanishi and Niino, 2009)		
Goddard (Tao et al., 1989)	Asymmetric convection model 2 (ACM2; Pleim, 2007)		
Thompson (Thompson et al., 2008)	Bougeault–Lacarrere (BouLac; Bougeault and Lacarrere, 1989)		
Milbrandt-Yau double-moment 7-class (MYDM7; Milbrandt and Yau, 2005)	University of Washington (UW; Bretherton and Park, 2009)		
Morrison double moment (Morrison; Morrison et al., 2009)	TEMF (Angevine et al., 2010)		
CAM double-moment 5-class (CAM; Eaton, 2011)	Shin-Hong scale-aware (Shin-Hong, Shin and Hong, 2015)		
Stony-Brook University (SBU; Lin and Colle, 2011)			
WRF double-moment 6-class (WDM6; Lim and Hong, 2010)			
NSSL double moment (NSSL2; Mansell et al., 2010)			

NSSL single-moment 7-class (NSSL1, Mansell et al., 2010)			
Aerosol-Aware Thompson (ThompsonAA; Thompson and Eidhammer, 2014)			
P3 (Morrison and Milbrandt, 2015)			

Table 2: List of default parameterization schemes for the simulation of outer domains (D01 and D02)

Parameterizations	D01	D02
Microphysics	SBU	SBU
Planetary boundary layer	Shin-Hong	Shin-Hong
Shortwave radiation	CAM	CAM
Longwave radiation	CAM	CAM
Culumus	Modifed Tiedtke (Tiedtke, 1989)	None
Land surface	Noah-MP	Noah-MP

640

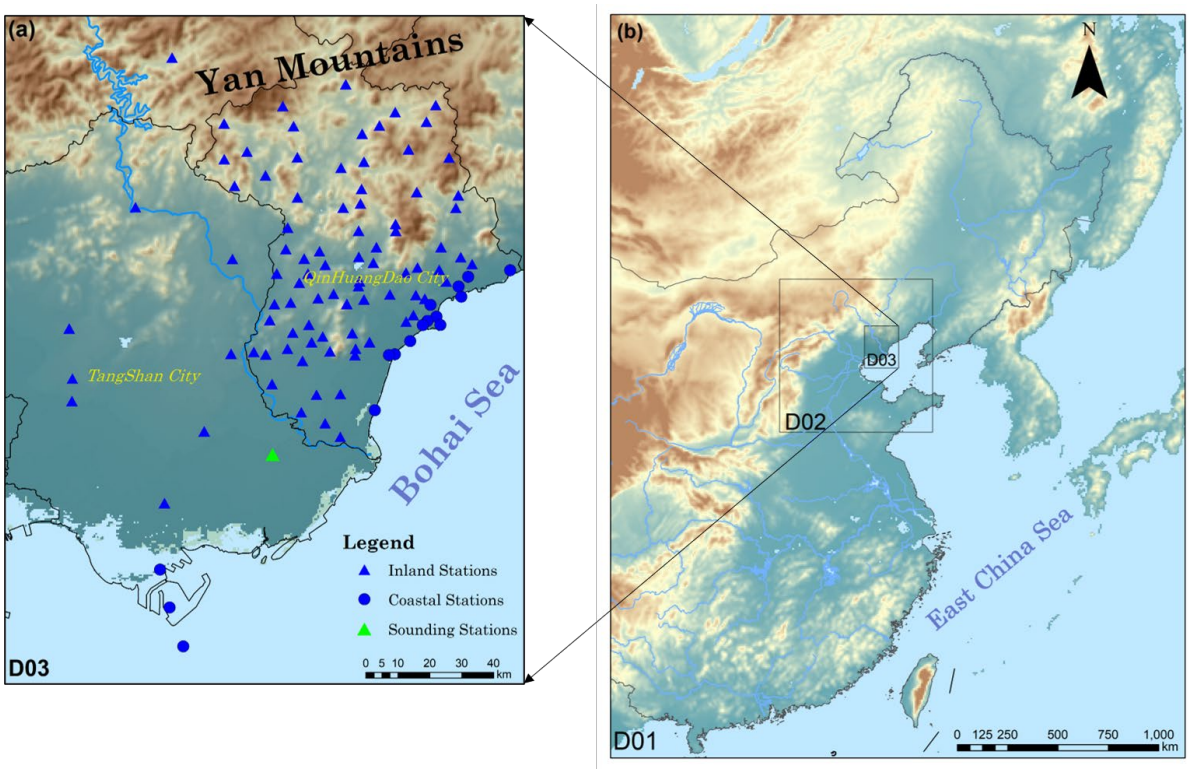

Figure 1: Map showing the (a) study area and (b) WRF nested domains (D01–D03). Solid blue circles and triangles in (a) represent coastal (16 stations in total) and inland stations (89 stations in total), and green triangle represent the sounding station.

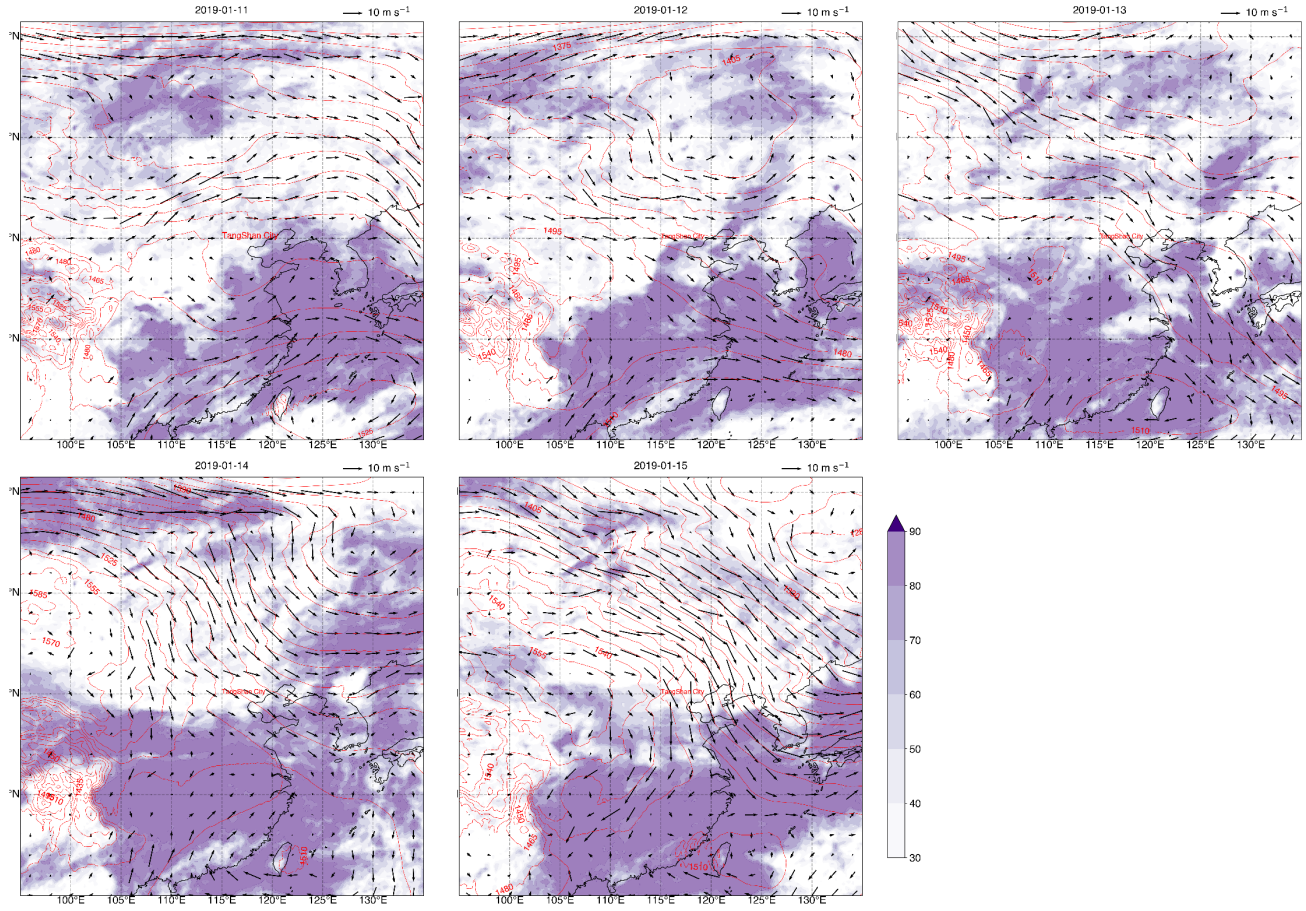

Figure 2: The daily averaged geopotential height (contour, units: gpm), winds (vectors, units: m/s) and cloud fraction (shading, units: %) at 925 hPa during 11 to 15 January 2019.

650

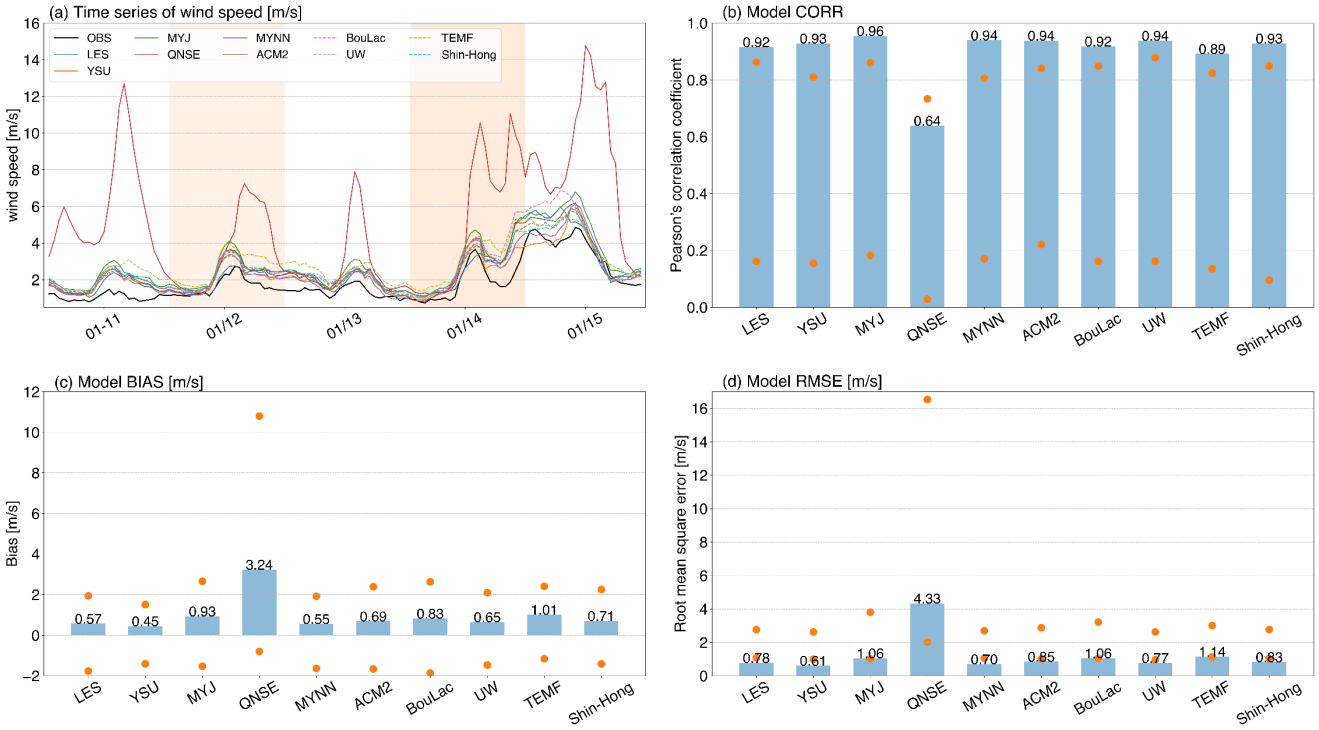

Figure 3: (a) Time series of observed and simulated wind speeds (m/s) and the corresponding statistics of (b) CORR, (c) BIAS and (d) RMSE for the PBL schemes. For each PBL scheme, the average is calculated over the 105 stations and then over all the simulations with that scheme, the dots in b, c and d represent the range across the stations.

655

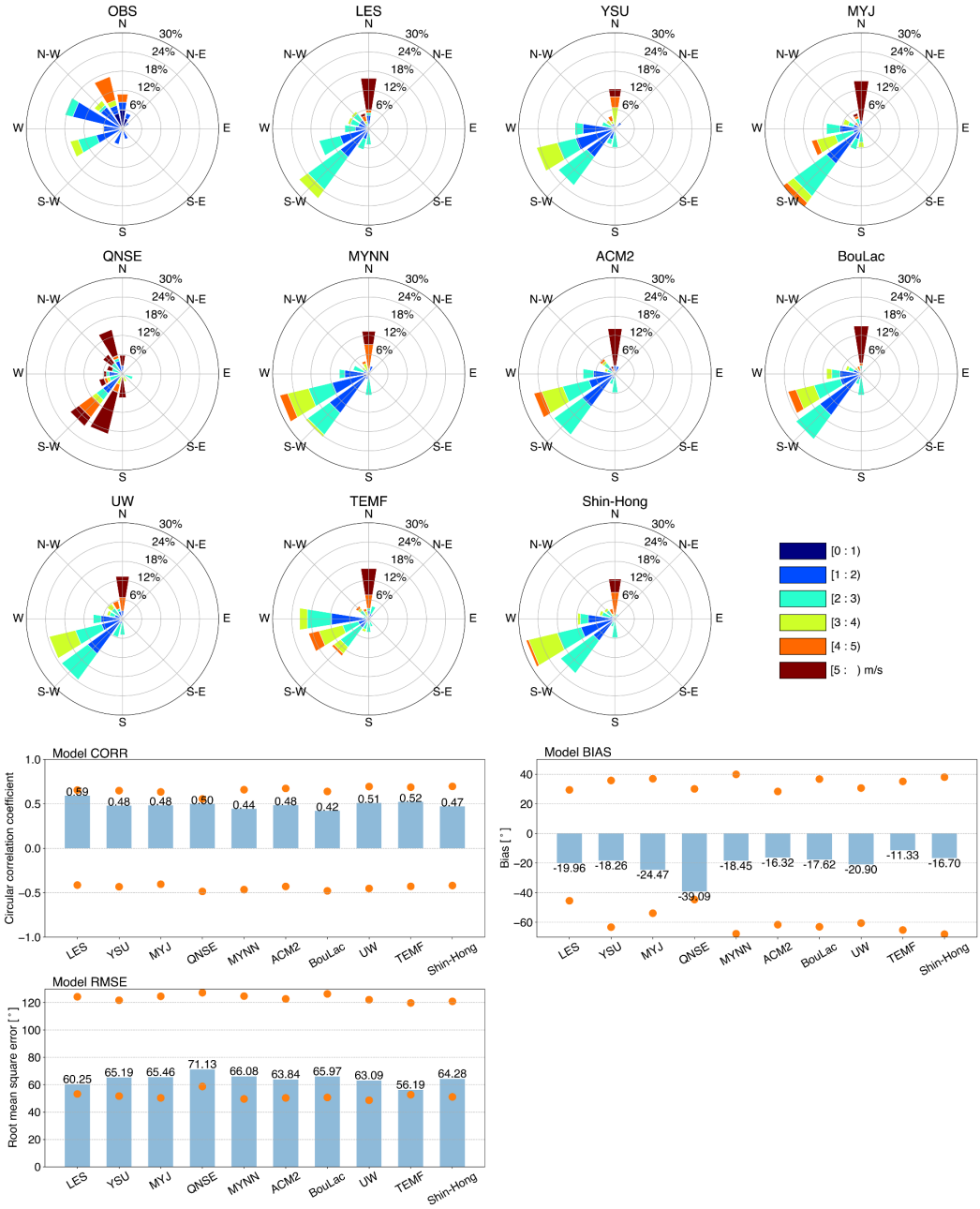

Figure 4: The wind rose charts for the PBL schemes during 11-15 January 2019 averaged over the stations and the corresponding scores of CORR, BIAS and RMSE, for each wind rose chart, the circles represent the relative frequency (%), and the colors represent wind speed (m/s).

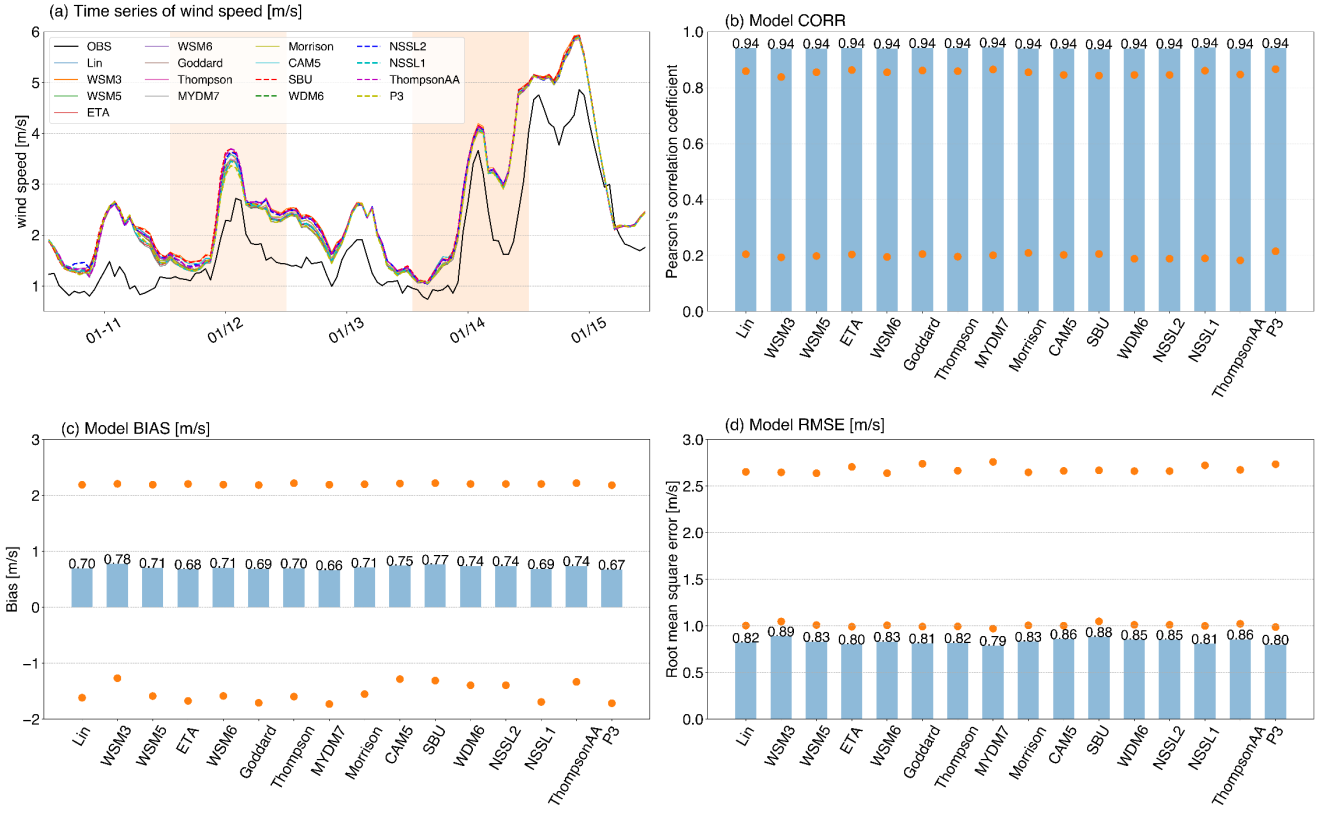

Figure 5: Same as Figure 3, but for the MP schemes.

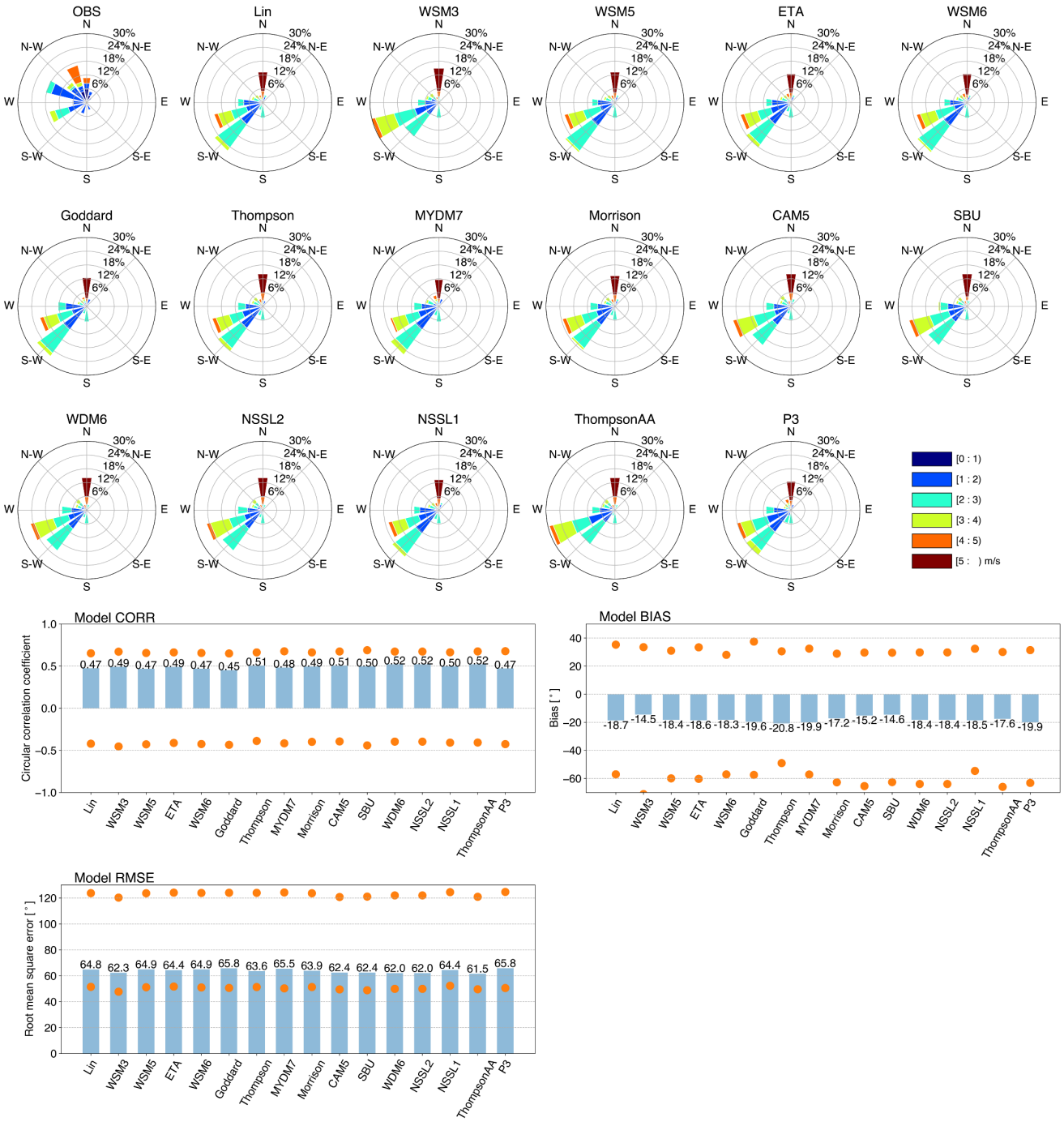

665 **Figure 6: Same as Figure 4, but for the MP schemes.**

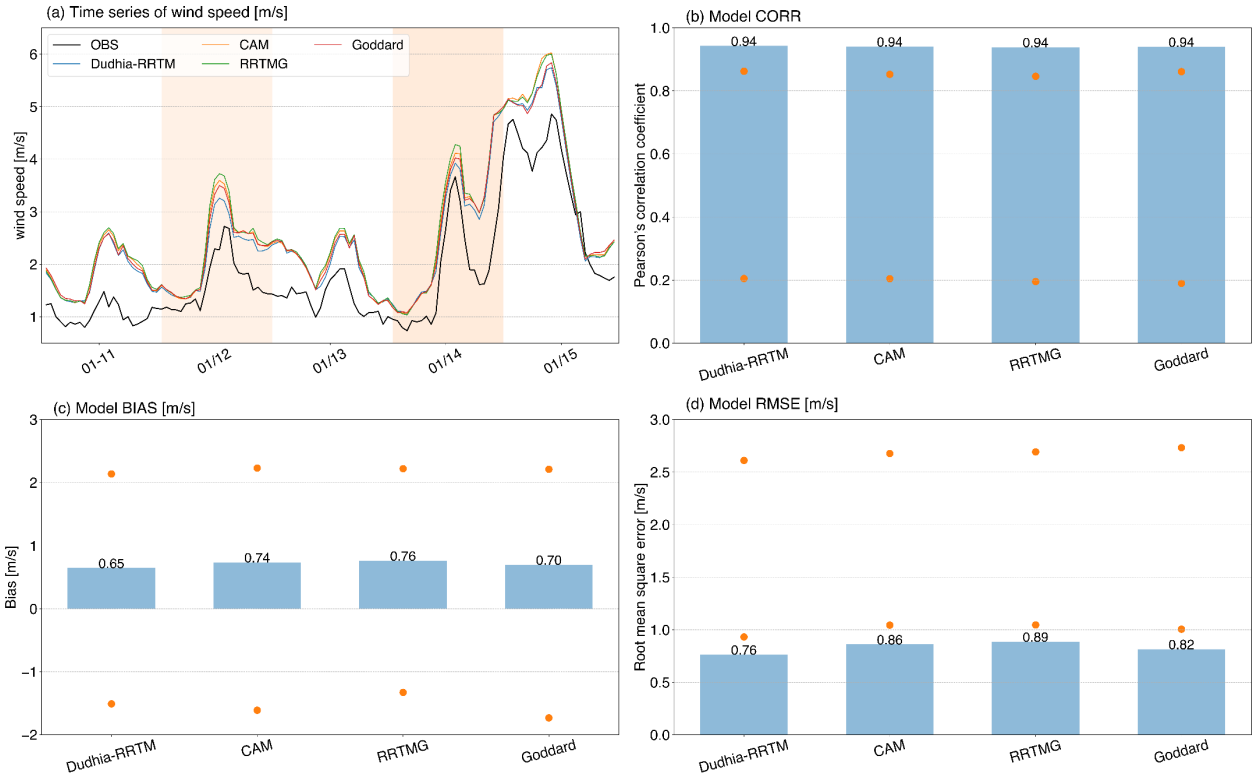

Figure 7: Same as Figure 3, but for the radiation schemes.

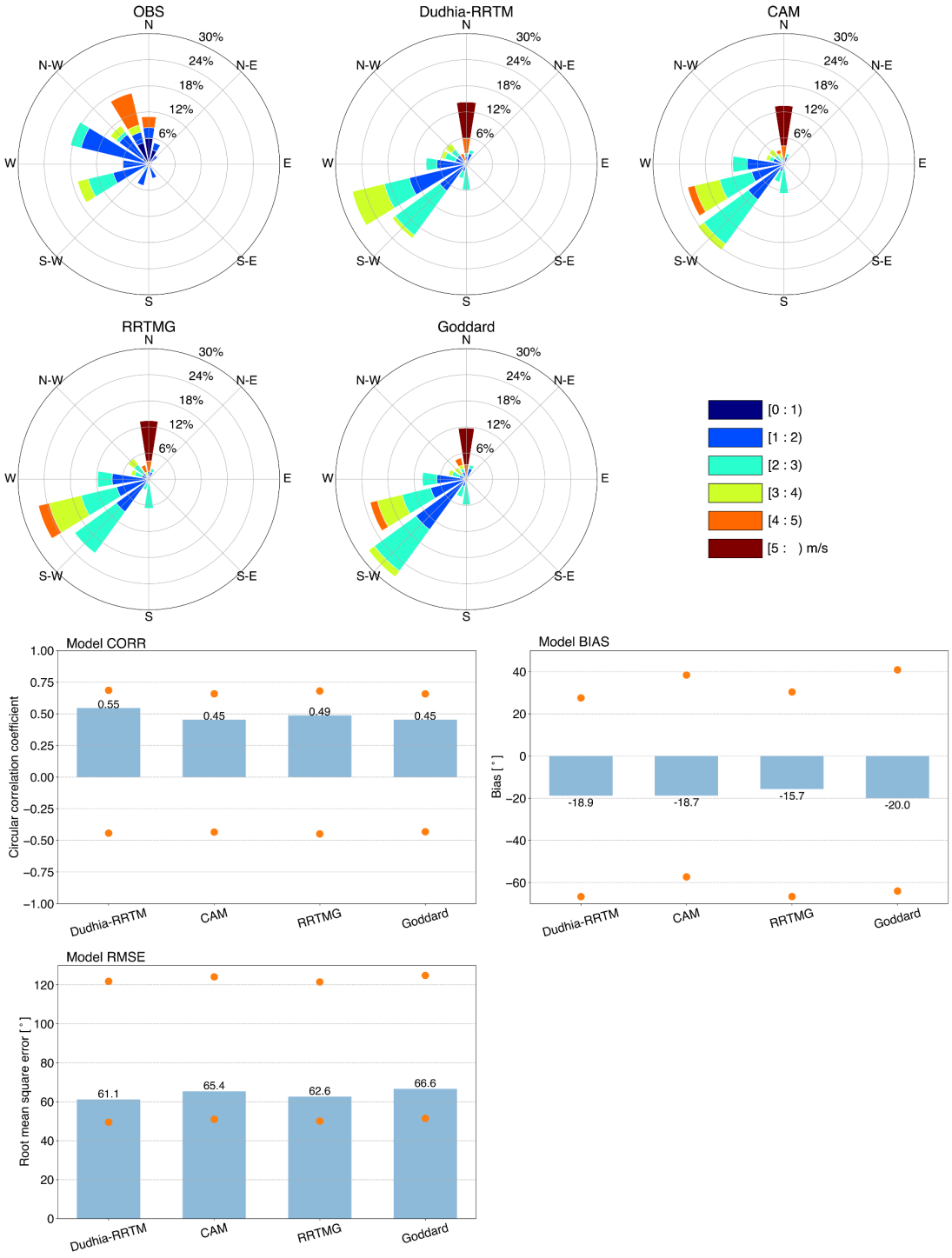

Figure 8: Same as Figure 4, but for the radiation schemes.

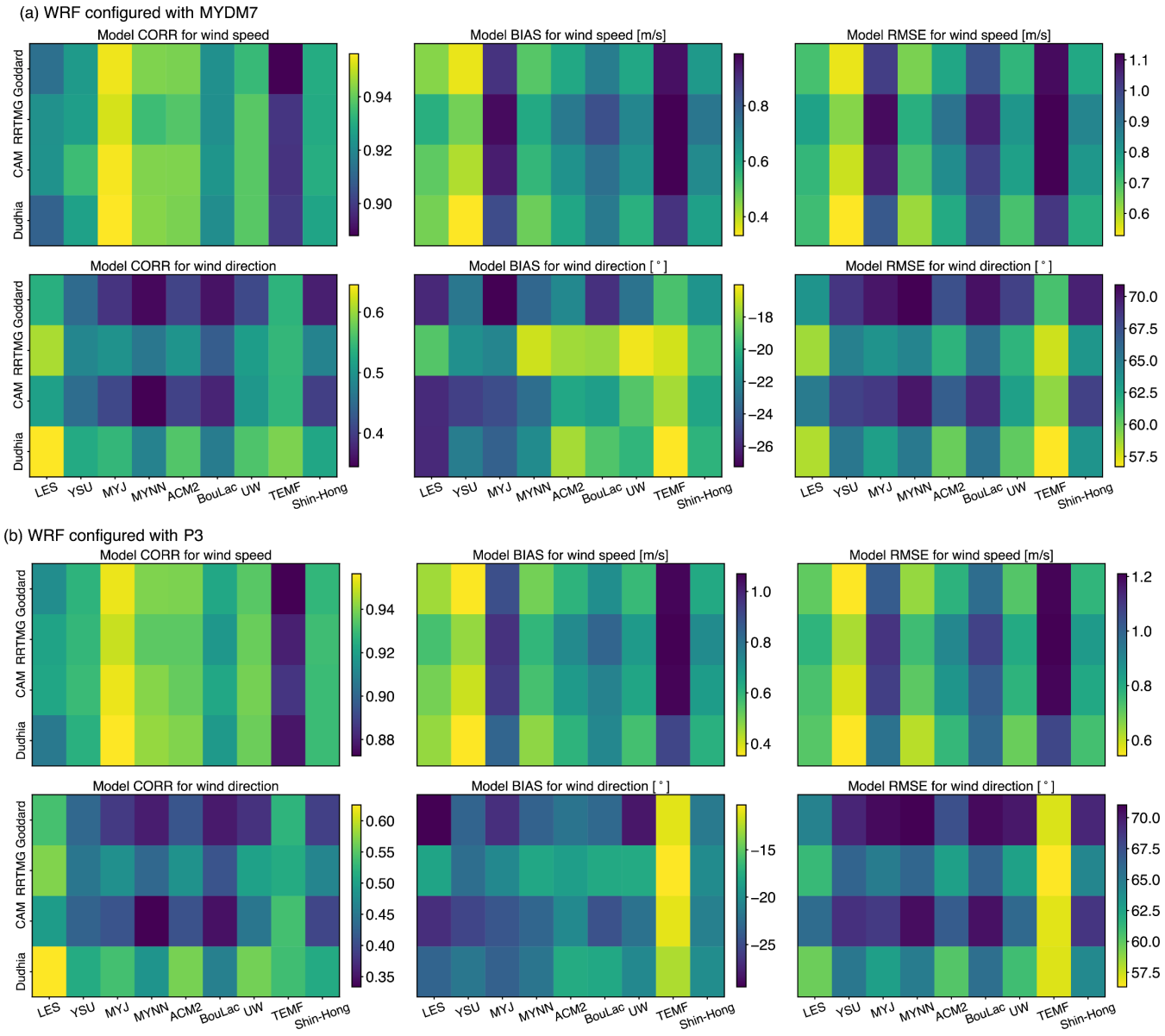

Figure 9: Statistic scores (CORR, BIAS and RMSE) for wind speed and direction for different combinations of PBL and radiation schemes. The MP schemes used are MYDM7 and P3.

675

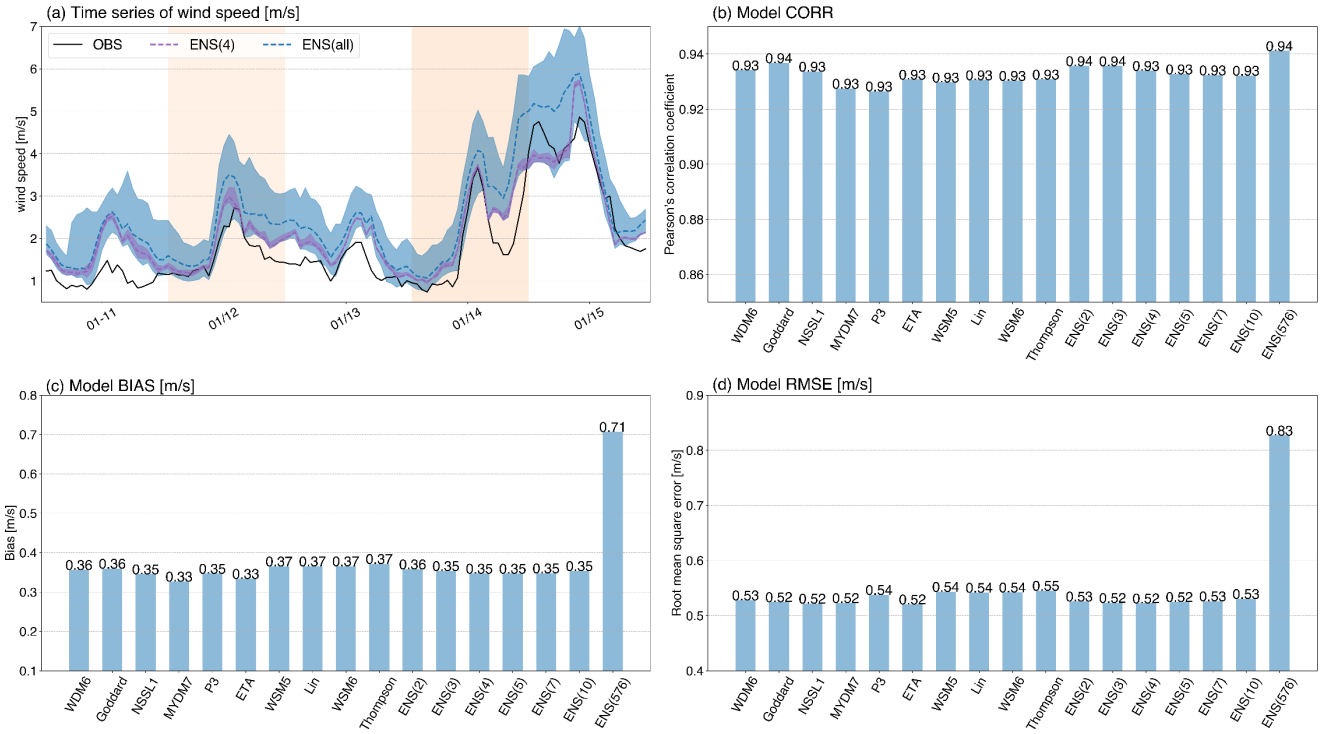

Figure 10: (a) Time series of wind speed (m/s) from observation and different ensembles, shading shows the spread, and the corresponding CORR, BIAS and RMSE scores are shown in b-d.

680

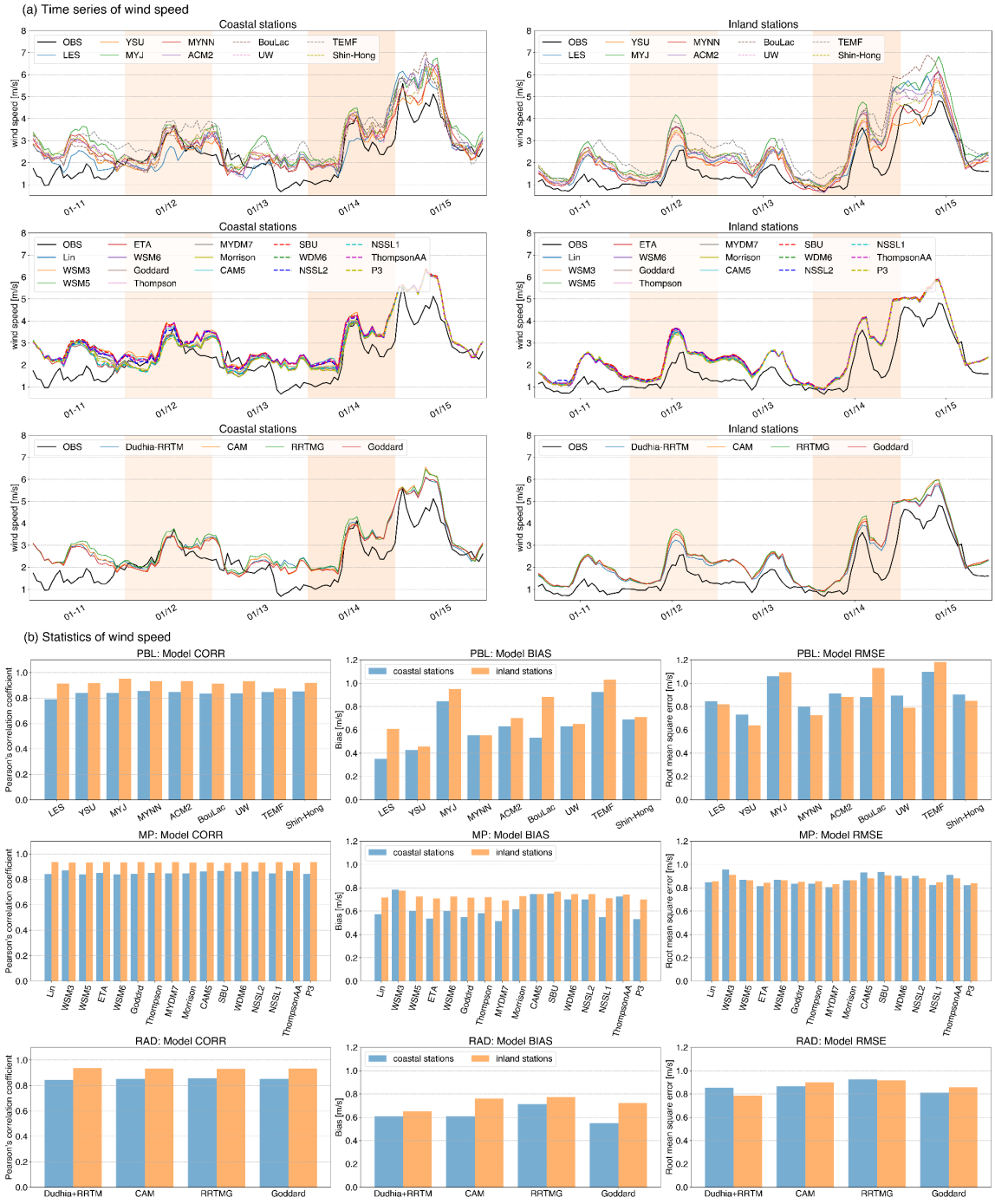

Figure 11: Comparison of simulated wind speeds between the coastal and inland stations shown in Figure 1a, as well as the corresponding statistic scores.

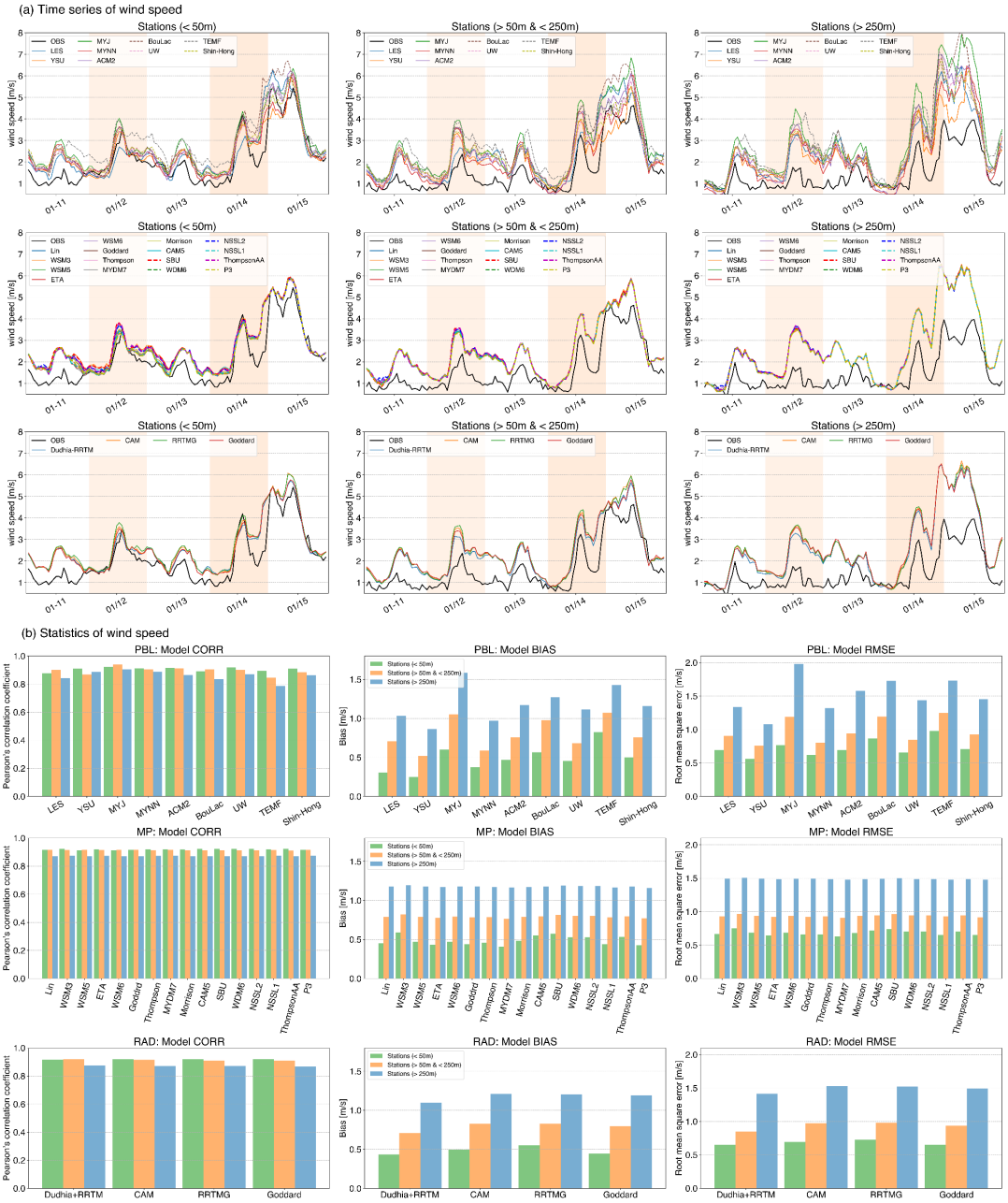

685 **Figure 12: Comparison of simulated wind speeds (m/s) for stations < 50m (51 stations in total), >50 & < 250m (36 stations in total) and < 250m (19 stations in total) and the corresponding statistic scores.**

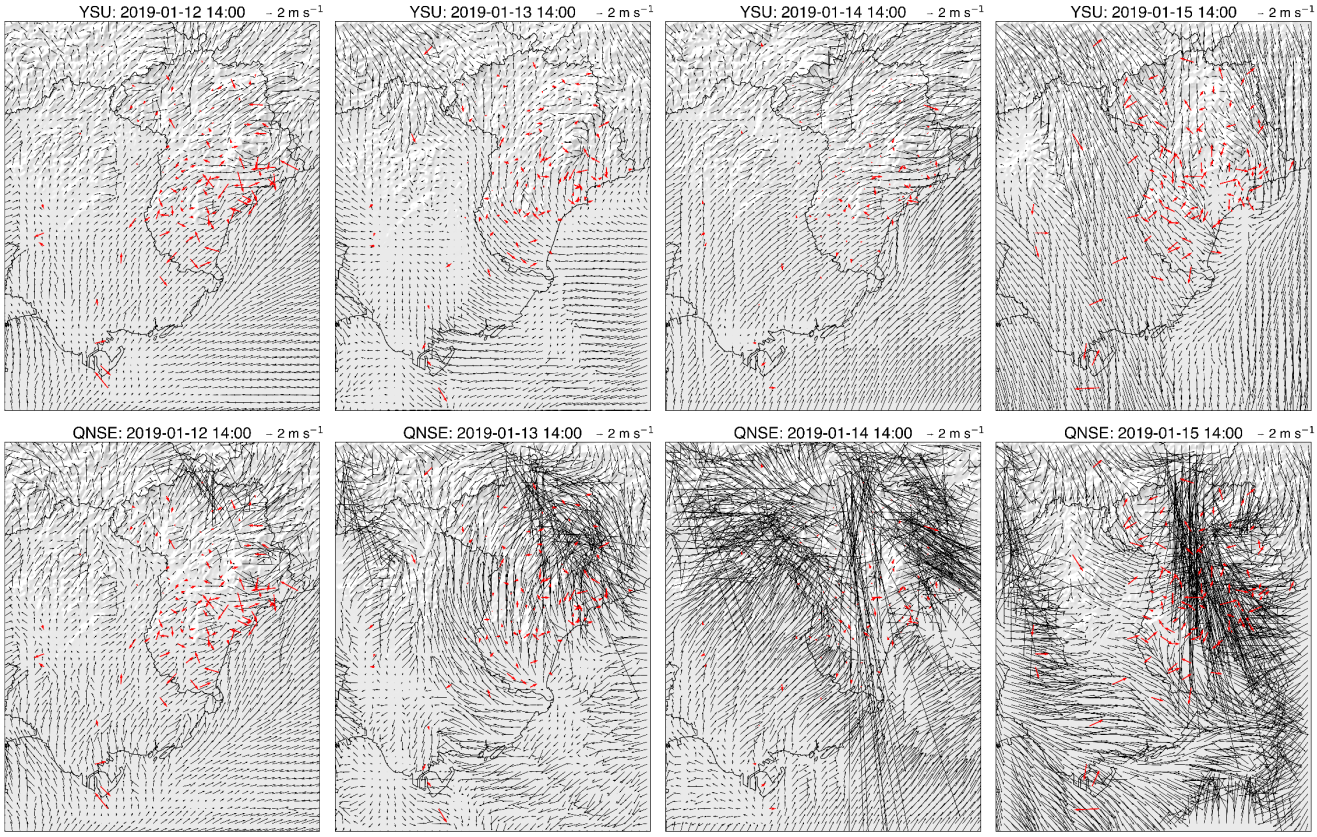

Figure 13: Spatial distribution of simulated (black vector) and observed (red vector) winds at 14:00 (in local time) during the study period from simulations with the YSU and QNSE schemes.

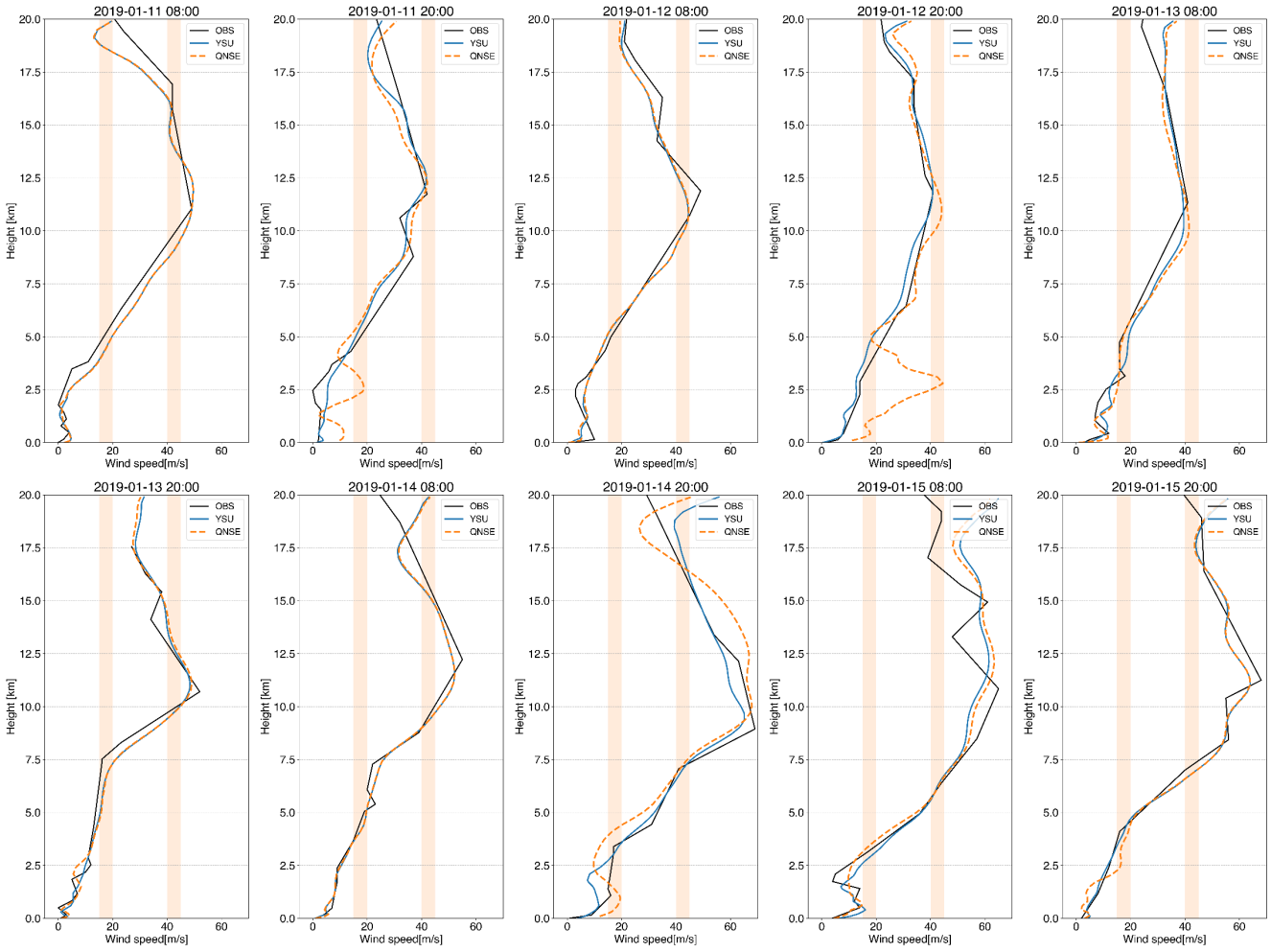

Figure 14: Wind speed profile from observation and simulations with the YSU and QNSE schemes at 08:00 and 20:00 (in local time) during the study period.

695

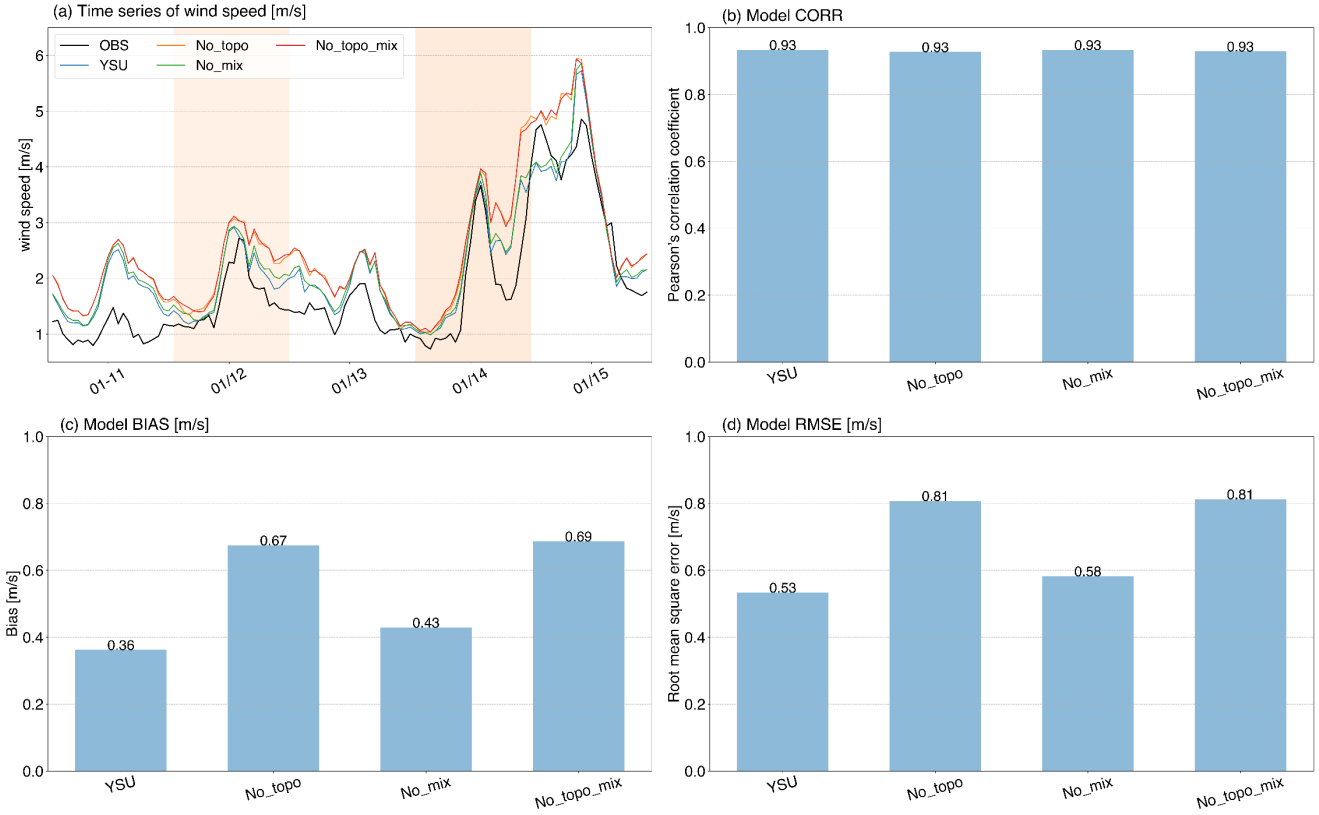

Figure 15: Same as Figure 3, but for simulations with different YSU options.

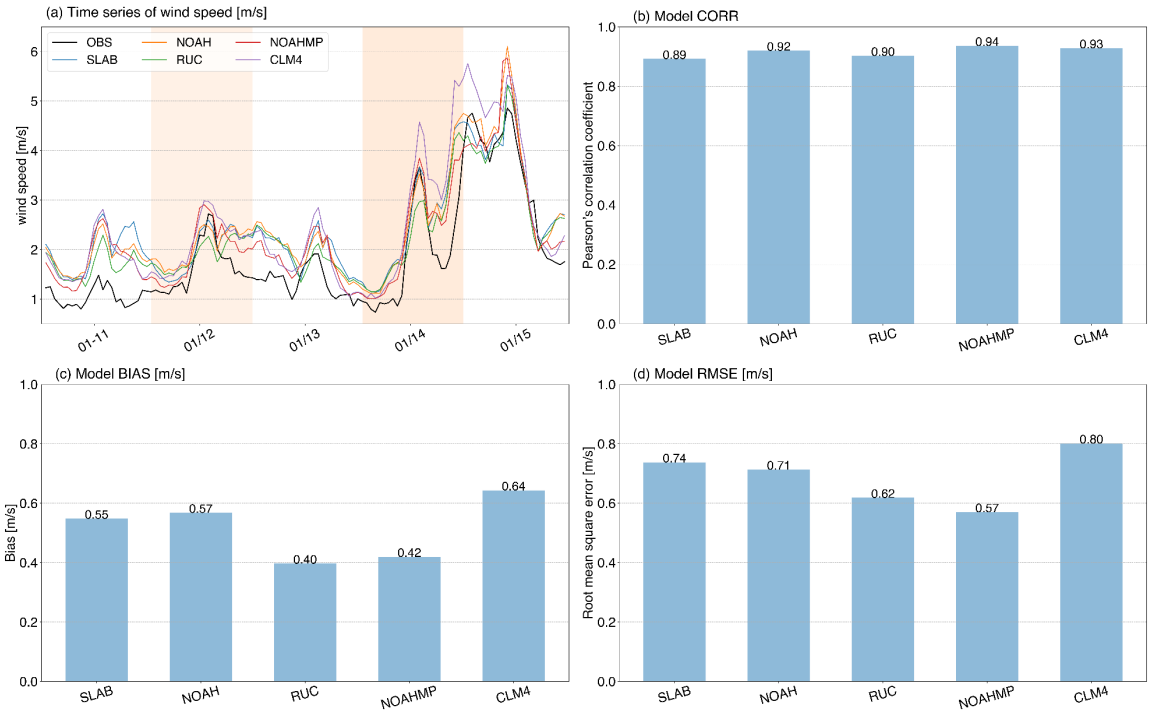

Figure 16: Same as Figure 3, but for simulations with different land surface schemes.